Experimental Thermal and Fluid Science 118 (2020) 110153

Contents lists available at ScienceDirect

Experimental Thermal and Fluid Science

journal homepage: www.elsevier.com/locate/etfs

Laminar hydrodynamic and thermal entrance lengths for simultaneously hydrodynamically and thermally developing forced and mixed convective flows in horizontal tubes

Marilize Everts, Josua P. Meyer*

Department of Mechanical and Aeronautical Engineering, University of Pretoria, Private Bag X20, Hatfield 0028, Pretoria, South Africa

ARTICLE INFO

Keywords:
Laminar
Entrance length
Constant heat flux
Simultaneously hydrodynamically and thermally developing, heat transfer, pressure drop

ABSTRACT

Correlations to predict the hydrodynamic and thermal entrance lengths in a smooth horizontal tube heated at a constant heat flux are often restricted to forced convection conditions. The reason being that most scholars do not distinguish very well between forced and mixed convection conditions. Furthermore, most correlations have been developed for hydrodynamically fully developed and thermally developing flows. The purpose of this study was to experimentally investigate the hydrodynamic and thermal entrance lengths for laminar flows in smooth horizontal tubes heated at a constant heat flux. Simultaneously hydrodynamically and thermally developing flows were investigated in both forced and mixed convection conditions. Two smooth circular test sections with inner diameters of 4 mm and 11.5 mm, and maximum length-to-diameter ratios of 1 373 and 872, respectively, were used. Heat transfer and pressure drop measurements were taken at Reynolds numbers between 460 and 3 200 at different heat fluxes. A large database with a total of 513 mass flow rate measurements, 43 501 temperature measurements, and 1 665 pressure drop measurements were used. The test fluid was water and the Prandtl number ranged between 3 and 8. For the first time, correlations were developed to calculate the hydrodynamic and thermal entrance lengths for simultaneously hydrodynamically and thermally developing flow in smooth horizontal tubes. The correlations were valid for tubes heated at a constant heat flux in both forced and mixed convection conditions. For ease of use, the correlations were developed in terms of the local, inlet, and bulk fluid properties. Furthermore, the mixed convection correlations were developed in terms of both the Grashof and modified Grashof numbers.

1. Introduction

A circular tube is the mathematically simplest circular geometry and is the most used geometry for tubes in internal fluid flow and heat transfer devices. Furthermore, compact heat exchangers are widely used owing to their small size and low cost. Owing to the small flow passages in these heat exchangers, the designed Reynolds number range is well within the laminar flow regime [1]. Most of these heat exchangers contain heat transfer surfaces, such as louvred and strip fin surfaces that interrupt the flow. This results in the development of new hydrodynamic and thermal boundary layers on the surface after each interruption, which leads to a higher heat transfer coefficient. Therefore, the hydrodynamic and thermal entrance lengths measured from a tube inlet are crucial parameters for design engineers, because they determine whether the velocity profile and heat transfer coefficients are dependent (developing flow) on or independent (fully developed flow) of the axial tube position.

In general, three types of laminar flows can develop through tubes. Fig. 1 depicts a schematic of the hydrodynamic and thermal boundary layers for these three types of flows, namely a (a) hydrodynamically developing isothermal flow, (b) hydrodynamically developing flow followed by a thermally developing flow, and (c) simultaneously hydrodynamically and thermally developing flow. As the fluid enters an isothermal tube (Fig. 1(a)), the fluid particles adjacent to the surface are slowed down owing to the no-slip velocity condition at the surface. Viscous effects cause this retardation effect to spread inwards. Furthermore, owing to continuity (constant cross-sectional mass flow rate) the slowed-down fluid near the surface causes the fluid in the centre to move faster. At the circumference along the tube, there exist developing hydrodynamic boundary layers, which increase in thickness along the tube length until the opposite sides merge in the centre of the tube. This location indicates the end of the inlet region [2]. However, an

* Corresponding author.
E-mail address: josua.meyer@up.ac.za (J.P. Meyer).

https://doi.org/10.1016/j.expthermflusci.2020.110153
Received 27 February 2020; Received in revised form 10 April 2020; Accepted 18 April 2020
Available online 23 April 2020

Nomenclature

A	Area
C	Coefficient used in correlations
C_p	Constant-pressure specific heat
D	Inner diameter
D_o	Outer diameter
EB	Energy balance error
f	Friction factor
g	Gravitational acceleration
Gr	Grashof number
Gr^*	Modified Grashof number
h	Heat transfer coefficient
I	Current
k	Thermal conductivity
L	Length
Lh	Hydrodynamic entrance length
Lt	Thermal entrance length
M	Measurement or calculated value
$\dot{m}$	Mass flow rate
n	Total
Nu	Nusselt number
P	Pressure
Pr	Prandtl number
$\dot{Q}_e$	Electrical input rate
$\dot{Q}_w$	Water heat transfer rate
$\dot{q}$	Heat flux based on $\dot{Q}_w$
R_{tube}	Tube thermal resistance
Re	Reynolds number
T	Temperature
V	Voltage
X	Distance from inlet

Greek letters

β	Thermal expansion coefficient
ε	Surface roughness
μ	Dynamic viscosity
ν	Kinematic viscosity
ρ	Density

Superscripts

–	Average
m, n, p	Exponents used in correlations

Subscripts

b	Bulk
c	Cross-section
cor	Correlation
exp	Experimental
FC	Forced convection
FD	Fully developed
i	Inlet
m	Mean
MC	Mixed convection
max	Maximum
o	Outer/outlet
s	Surface

important note is that, although the hydrodynamic boundary layers merge, the velocity profile continues to develop. As indicated by the dotted blue line in Fig. 1(a), the hydrodynamic entrance length is considered to be the tube length required for the centreline velocity to attain 99% of the fully developed value [3] or the friction factor values to be within 5% of the fully developed friction factor values [4].

When heat is applied to the surface of a tube (for example, a tube heated at a constant heat flux), the fluid particles adjacent to the surface reach the temperature of the surface. This results in the temperature of the fluid near the surface being different from the fluid near the centreline of the tube. This temperature difference inside the tube leads to convection heat transfer in the radial direction and the development of a thermal boundary layer. The thickness of the thermal boundary layer increases along the tube length until the opposite sides merge in the centre of the tube. Note that for the case in Fig. 1(b), the flow is already hydrodynamically fully developed before the tube is heated and the thermal boundary layers begin to develop. However, in Fig. 1(c), the entire tube is heated; therefore, the hydrodynamic and thermal boundary layers develop simultaneously. As indicated by the dotted red line in Fig. 1, Siegel *et al.* [5] defined the thermal entrance length for laminar flow as the heated length required for the Nusselt number to be within 5% of the theoretical fully developed value of 4.36 for a constant heat flux boundary condition.

The Prandtl number is the ratio of the kinematic viscosity (diffusion rate of momentum) to the thermal diffusivity (diffusion rate of heat) and provides an indication of the development of the hydrodynamic and thermal boundary layers. For Prandtl numbers greater than 1 (which is the case for most fluids), the viscous effects diffuse faster; therefore, the hydrodynamic boundary layer is shorter than the thermal boundary layer (Fig. 1(b)), while the opposite is true for Prandtl numbers smaller than 1 (which is the case for most gases).

Owing to its importance, the hydrodynamic entrance length has been investigated since as early as 1891. It was initially referred to as the 'transition length' because the flow was considered to be transitioning to a fully developed laminar flow. Bodoia and Osterle [6] referred to the hydrodynamic entrance length more clearly as the development length in 1961, and, since 1963 [7], researchers have referred to it as the 'entrance length' in articles and textbooks.

Boussinesq [8] first investigated the hydrodynamic entrance length analytically in 1891, and since then, approximately 26 analytical, numerical, and experimental studies focused specifically on the hydrodynamic entrance length in horizontal circular tubes. The majority (11) of these studies were performed analytically (Table 1) by linearizing the inertia terms or using integral methods. Table 2 provides a summary of nine numerical investigations that utilized either the finite difference, finite element, or finite volume solution of the boundary layer equations. To date, only seven experimental investigations (Table 3) focussed on the hydrodynamic entrance length of a Newtonian fluid flowing through a smooth horizontal circular tube.

According to most authoritative fluid mechanics textbooks [29–37], the forced convection hydrodynamic entrance length, Lh_{FC}, can be calculated using

$$Lh_{FC} \approx 0.06ReD \tag{1}$$

where Re is the Reynolds number, and D is the inner diameter of the tube in which the fluid flows. However, as noted by Durst *et al.* [25], a lot of contradicting data for the hydrodynamic entrance length have been reported. Table 1 indicates that analytical investigations yielded coefficients between 0.026 and 0.086, while the coefficients obtained from numerical and experimental investigations varied between 0.055 and 0.088 (Table 2) and between 0.034 and 0.09 (Table 3), respectively. Therefore, the difference in the coefficients obtained by different investigations was due to the different assumptions, methods, and criteria that were used.

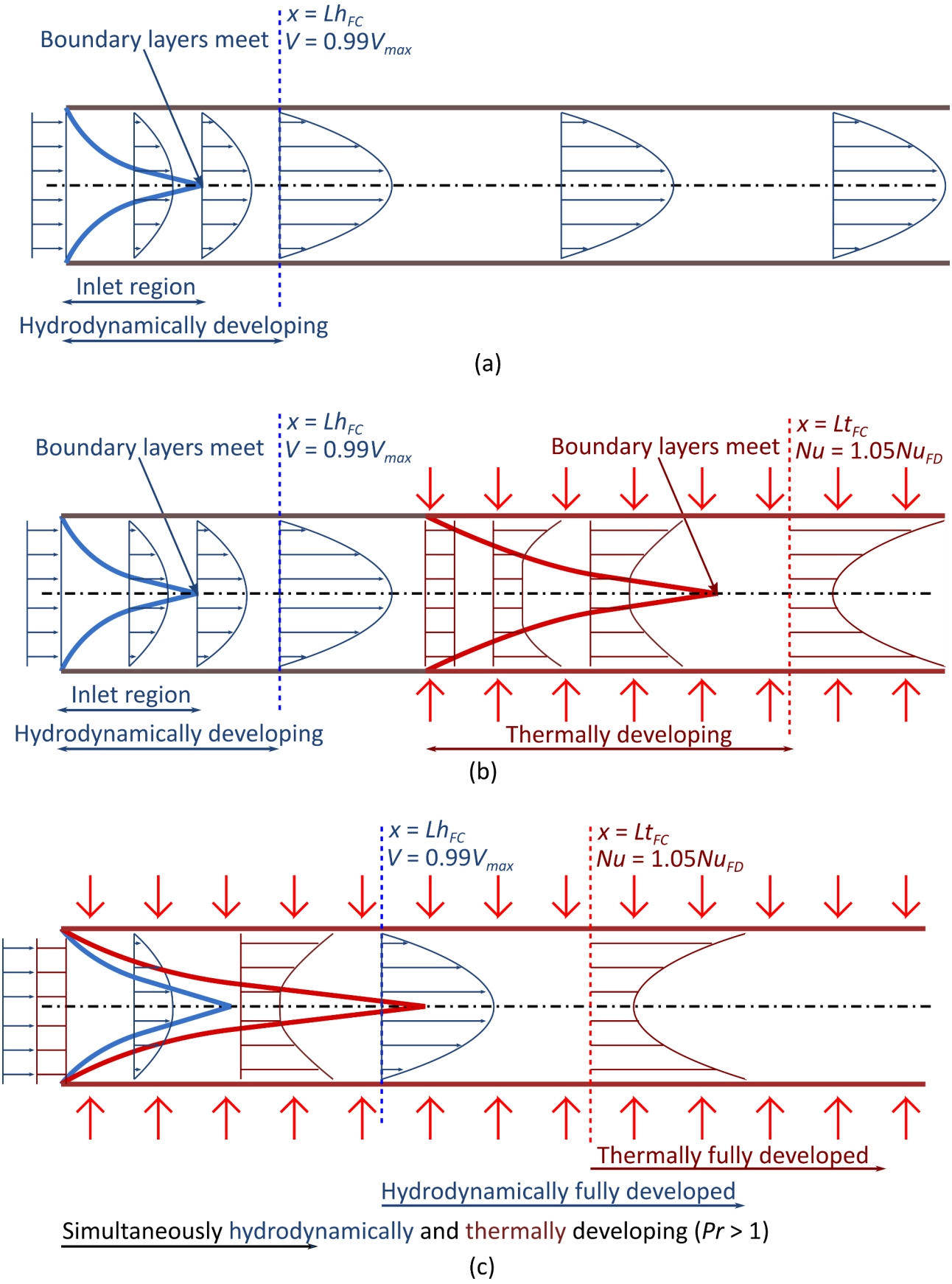

Fig. 1. Schematic of the hydrodynamic and thermal boundary layers and entrance lengths for a (a) hydrodynamically developing isothermal flow, (b) hydrodynamically developing flow followed by thermally developing flow, and (c) simultaneously hydrodynamically and thermally developing flow. Temperatures are not vectors (length is an indication of temperature).

Table 1
Summary of analytical results of studies that focused on the laminar hydrodynamic entrance length in horizontal circular tubes.

Study	Year	Inlet velocity profile	Assumptions/comments	Criteria	Lh/D	Range
Boussinesq [8]	1891	Uniform	Linearization of inertia terms	Centreline 99% of V_{max}	$0.065Re$	Not specified
Langhaar [9]	1942	Uniform	Linearization of inertia terms; fairly rapid spread of viscous effects into the bulk fluid through velocity profiles outside the boundary layer	Centreline 99% of V_{max}	$0.058Re$	Not specified
Schiller [10]	1922	Uniform	Integral method; parabolic velocity profile in the boundary layer; neglect viscous dissipation in the boundary layer	Boundary layers meet in the centre of the tube	$0.029Re$	Not specified
Siegel [11]	1953	Uniform	Integral method; cubic and quartic velocity profile in the boundary layer; neglect viscous dissipation in the boundary layer	Boundary layers meet in the centre of the tube	$0.03Re$	Not specified
Campbell & Slattery [7]	1963	Uniform	Integral method; parabolic velocity profile in the boundary layer; account for viscous dissipation in the boundary layer	Centreline 99% of V_{max}	$0.068Re$	Not specified
McComas [12]	1967	Uniform	Integral method; neglect viscous dissipation in the boundary layer; only deal with inviscid flows along the centreline	Boundary layers meet in the centre of the tube	$0.026Re$	Not specified
Fargie & Martin [13]	1971	Uniform	Integral method	Centreline 99% of V_{max}	$0.049Re$	Not specified
Chen [14]	1973	Uniform	Integral method; parabolic velocity profile in the boundary layer; no boundary layer assumptions	Centreline 99% of V_{max}	$0.72/(0.04Re + 1) + 0.061Re$	Not specified
Mohanty & Asthana [2]	1978	Uniform	Integral method	Average 99% of V_{max}	$0.075Re$	$Re > 500$
Matras & Stachura [15]	1981	Uniform	Integral method	Average 99% of V_{max}	$0.0864Re$	$Re > 500$
Du Plessis & Collins [16]	1992	Uniform	Mathematical analysis using the method by Churchill & Usagi [17]	Product of the friction factor and the Reynolds number	$0.0462Re$	Not specified

Table 1 indicates that the investigations [10–12] that considered the flow to be hydrodynamically fully developed when the boundary layers merged in the centre of the tube yielded coefficients between 0.026 and 0.03. However, the investigations that considered the flow to be hydrodynamically fully developed when the centreline velocity was 99% of the maximum velocity yielded significantly larger coefficients that varied between 0.049 and 0.0675. Furthermore, two investigations [2,15] that only considered the flow to be hydrodynamically fully developed when the average velocity was 99% of the maximum velocity yielded even larger coefficients of 0.075 and 0.086. According to Mohanty and Asthana [2], the laminar hydrodynamic boundary layers merge in the centre of the tube much earlier than when the velocity is 99% of the maximum velocity. This would explain why significantly smaller coefficients (approximately 0.03) were obtained when the flow was considered to be fully developed once the boundary layers merged.

While the majority of studies used the centreline velocity as a criterion for hydrodynamically fully developed flow, Mohanty and Asthana [2] employed the average velocity because the centreline velocity cannot be assessed independently, e.g. using Bernoulli's equation. This, however, led to higher coefficients. Shah and Bhatti [38] also noted that the coefficients are dependent on the approximations made. The boundary-layer theory simplifications (negligible axial momentum diffusion and radial pressure variation) yielded a single coefficient, similar to Eq. (1). Note that boundary-layer theory simplifications are justified by order of magnitude considerations for high Reynolds numbers, while laminar flow is associated with low Reynolds numbers [39]. Chen [14], who made no boundary layer assumptions, therefore obtained a Reynolds number dependent coefficient, $C = 0.061 + 0.72/[Re(1 + 0.04Re)]$.

Most of the coefficients obtained from numerical investigations (Table 2) were approximately 0.056. However, some investigations [20,21,23] obtained different coefficients for different Reynolds numbers, especially when the Reynolds numbers were smaller than 150. This was due to axial diffusion, which became significant at very small Reynolds numbers [22,40]. Atkinson *et al.* [22] obtained the following correlation that is valid for Reynolds numbers between 1 and 1 000:

$$Lh_{FC} = (0.59 + 0.056Re)D \tag{2}$$

To improve the accuracy of the hydrodynamic entrance length, specifically between Reynolds numbers of 1 and 100, Durst *et al.* [25] numerically obtained the following correlation:

$$Lh_{FC} = [0.619^{1.6} + (0.0567Re)^{1.6}]^{1/1.6}D \tag{3}$$

When comparing the results of the experimental investigations (Table 3) with those of the analytical (Table 1) and numerical (Table 2) investigations, it is clear that the available experimental data is very limited. Although the first experiments were conducted by Nikuradse [27] as early as 1934, the original data points, the fluid used, and a description of the experimental method used have not been reported [7,13,19,39,41,42]. Apart from the unpublished experimental investigation conducted by Nikuradse, the only other experimental investigations that specifically focussed on the hydrodynamic entrance length of Newtonian fluids through horizontal circular tubes, were conducted in the 1960s and 1970s. These studies typically investigated the hydrodynamic entrance length at two to six different Reynolds numbers only. It should therefore be noted that the total number of experimental cases (different Reynolds numbers) in literature at which the hydrodynamic entrance length was investigated is *only* approximately 18.

The results of the experimental investigations listed in Table 3 indicate that coefficients of 0.52–0.56 were obtained when the flow was considered to be hydrodynamically fully developed when the centreline velocity was 99% of the maximum velocity. Similar to the analytical results in Table 1, a larger coefficient was obtained when the average velocity was used as the criterion. From their results, Emery and Chen [43] concluded that a much shorter entrance length (coefficient of

Table 2
Summary of numerical results of studies that focused on the laminar hydrodynamic entrance length in horizontal circular tubes.

Study	Year	Inlet velocity profile	Assumptions/comments	Criteria	Lh/D	Range
Hornbeck [18]	1964	Uniform	Finite difference solution of boundary layer equations	Centreline 99% of V_{max}	$0.0565Re$	$Re > 200$
Christiansen & Lemmon [19]	1965	Uniform	Finite difference solution of boundary layer equations	Centreline 99% of V_{max}	$0.0555Re$	$200 < Re < 500$
Vrentas *et al.* [20]	1966	Streamtube	Finite difference solution of boundary layer equations	Centreline 99% of V_{max}	$(0.0535–0.33)Re$ $0.0563Re$	$Re = 1, 50, 150$ $Re \geq 250$
Friedman *et al.* [21]	1968	Uniform	Finite difference solution of boundary layer equations	Centreline 99% of V_{max}	$(0.061–0.088)Re$ $0.0565Re$ $0.056Re$	$Re = 10, 20, 40$ $Re = 100, 150, 200$ $Re \geq 300$
Atkinson *et al.* [22]	1969	Uniform	Finite element solution of boundary layer equations	Centreline 99% of V_{max}	$0.59 + 0.056Re$	$1 < Re < 1\,000$
Pagliarini [23]	1989	Uniform	Finite element solution of boundary layer equations	Centreline 99% of V_{max}	$(0.054–0.385)Re$ $0.055Re$	$Re = 1, 5, 50$ $Re \geq 150$
Nguyen [24]	1993	Uniform	Finite difference solution of boundary layer equations	Centreline 99% of V_{max}	$0.02519 + 0.3572/Re$ $0.0555Re$	$1 < Re < 10$ $Re > 20$
Durst *et al.* [25]	2005	Uniform	Finite volume solution of boundary layer equations	Centreline 99% of V_{max}	$[(0.619)^{1.6} + (0.0567Re)^{1.6}]^{1/1.6}$	$0.1 < Re < 4\,000$
Joshi & Vinoth [26]	2018	Streamtube	Finite volume solution of boundary layer equations	Centreline 99% of V_{max}	$-0.0437 + 0.0553Re + 0.413e^{-0.1Re}$	$0.001 < Re < 4\,000$

0.03) was observed based on the pressure gradient than on the centreline velocity (coefficient of 0.0625). Lienhard and Lienhard [4] also noted that a coefficient of 0.03 ensures that the friction factor values are within 5% of the fully developed laminar friction factor values, while a coefficient of 0.05 ensures that they are within 1.4%. Although a sharp-edged entrance was expected to have a reduced entrance length [43,44], the results in Table 3 indicate that the fully developed flow criterion had a greater influence on the coefficients than the inlet geometry.

Despite the wide range and different forms of the hydrodynamic entrance length, most of the authoritative fluid mechanics textbooks still use Eq. (1) to calculate it. However, it is interesting to note that fluid mechanics textbooks [29–37] present a coefficient of 0.06, while heat transfer textbooks [3,45–49] present a coefficient of 0.05. Furthermore, Eq. (1) does not consider heating (the simultaneous development of the hydrodynamic and thermal boundary layers) and thus is valid for isothermal tubes only.

According to most authoritative heat transfer textbooks [3,45–49], the forced convection thermal entrance length, Lt_{FC}, is the product of the hydrodynamic entrance length, Lh_{FC}, with the Prandtl number, Pr:

$$Lt_{FC} = Lh_{FC}Pr = 0.05RePrD \tag{4}$$

However, similar to the hydrodynamic entrance length, there is an uncertainty on the value of the coefficient. Furthermore, it is unfortunate that it is not emphasized in heat transfer textbooks that Eq. (4) is not valid for mixed convection conditions, but only forced convection conditions. While fluid mechanics and heat transfer textbooks use coefficients of 0.06 and 0.05, respectively, they do not give information on the influence of boundary and flow conditions (such as constant heat flux or constant surface temperature, hydrodynamically fully developed or developing, or inlet geometry). Table 4 provides a summary of the analytical and numerical investigations that used a constant heat flux boundary condition. To the authors' best knowledge, no experimental investigations specifically focussed on the thermal entrance length of laminar flow through a horizontal tube heated at a constant heat flux. Several experimental investigations focussed on laminar developing flow through horizontal tubes heated at a constant heat flux; however, the focus was on the local heat transfer coefficients and not on the thermal entrance length.

Table 4 indicates that the investigations [5,23,40,50,51] that considered hydrodynamically fully developed and thermally developing flow yielded a coefficient of approximately 0.043. According to Lienhard and Lienhard [4], the coefficient can vary between 0.028 and 0.053, depending on the Prandtl number and the wall boundary conditions when the hydrodynamic and thermal boundary layers develop simultaneously. Specifically, for a constant heat flux boundary condition the coefficient can vary between 0.042 and 0.053 depending on the Prandtl number [38].

Table 4 also clearly indicates that only six investigations [5,23,24,40,50,51] focused on the thermal entrance length of Newtonian fluids flowing through smooth horizontal tubes with a constant heat flux boundary condition. Furthermore, almost all of them considered hydrodynamically fully developed and thermally developing flows (Fig. 1(b)). To the best of our knowledge, only Nguyen [24] considered simultaneously hydrodynamically and thermally developing flows. From the experimental data of Roy [52], Bergles and Simonds [53] predicted that the thermal entrance length might be longer when the flow is simultaneously hydrodynamically and thermally developing; the authors did not explain the physics of the phenomenon or the rationale of their prediction. However, this is indeed confirmed when comparing the coefficients of hydrodynamically fully developed [40] and simultaneously developing flows [24].

Furthermore, the investigations summarised in Table 4 considered forced convection heat transfer only, while almost all practical applications involve mixed convection conditions. Newell [39] concluded, from an order of magnitude comparison of the four types of forces (viscous, pressure, body and inertia forces) present in fluid motion, that forced convection conditions will only exist in the laminar flow regime if the tube diameters are very small, the heat flux is very low or the β/ν-ratio is very large. From the large experimental database of Meyer and Everts [54], it was found that only 5.4% of their 891 fully developed laminar experimental data points contained forced convection conditions (fully developed Nusselt numbers within 5% of the theoretical fully developed Nusselt number of 4.36 for a constant heat flux boundary condition). Therefore, 95% of their experimental data (which is the largest database published thus far in open literature) involved mixed convection and not forced convection.

When heat is applied to the tube surface, the fluid near the surface (which has a higher temperature and thus a lower density) circulates upward along the tube surface. Continuity then requires the fluid in the centre of the tube (which has a lower temperature and higher density) to flow downward. This leads to a secondary fluid motion, which is symmetrical about a vertical plane and is also known as free convection effects. Combining the secondary fluid motion with the axial fluid velocity leads to three-dimensional streamlines with a spiralling character [55]. Although free convection effects are always present when a

Table 3
Summary of experimental results of studies that focused on the laminar hydrodynamic entrance length in horizontal circular tubes.

Study	Year	Inlet velocity profile	Method	Test Fluid	Criteria	Lh/D	Range	Number of cases
Nikuradse [27]	1934	Bellmouth	Not specified	Not specified	Not specified	$0.0625Re$	Not specified	
Brocklebank & Smith [28]	1968	Uniform	Point liquid velocities from stroboscopic streak photographs	Glycerol	Centreline 99% of V_{max}	$0.55 + 0.056Re$	Re = 1.16, 3.3, 6.34, 23.4	4
Emery & Chen [43]	1968	Sharp-edged inlet	Static pressures measured at 21 locations using vertical manometers; centreline velocities measured with modified Cole pitometer and manometer	Ethylene glycol ($Pr \approx 200$)	Centreline 99% of V_{max} 95% of dP/dx	$0.052Re0$ $0.034Re$	Re = 1 200, 2 600	2
Atkinson *et al.* [22]	1969	Uniform	Point velocities determined using optical technique	Water	Centreline 99% of V_{max}	$0.59 + 0.056Re$	Re = 1.1, 3.3, 6.3, 23.2, 109, 215	6
Fargie & Martin [13]	1971	Abrupt contraction	Centreline velocities obtained from pitot tube traverses in conjunction with wall static pressure measurements	Mobiltherm ($Pr \approx 1\,520$)	Centreline 99% of V_{max}	$(0.052–0.068)Re$	Re = 760, 1 229, 1 512	3
Mohanty & Asthana [2]	1978	Short bellmouth	Velocity field traverse obtained from microprobe in conjunction with an Askania micromanometer	Air	Average 99% of V_{max}	$0.075Re$	Re = 1 875, 2 500, 3 250	3
Total								**18**

temperature difference exists inside a tube, they are not always significant compared with the axial fluid velocity. The flow regime maps developed by Metais and Eckert [56] for a constant surface temperature boundary condition and by Everts and Meyer [57] for a constant heat flux boundary condition, can be used to determine whether free convection effects are negligible (forced convection) or significant (mixed convection).

Mixed convection conditions can increase the heat transfer to a fluid in laminar flow through a horizontal tube by a factor of three or four [58]; therefore, free convection effects have a significant influence on the flow characteristics. To account for mixed convection, Hallman [59] defined the thermal entrance length as the point where the experimental curve of the local Nusselt numbers, as a function of the axial position crosses, merges, or becomes parallel to the constant-property solution (Nu_{FC} = 4.36) provided by Siegel *et al.* [5]. However, this definition might lead to inaccurate results, as observed from experiments using air by McComas and Eckert [60], at high Grashof numbers and low Reynolds numbers. The local Nusselt numbers do not continue to decrease along the tube length until they become fully developed and constant. In the experiments of McComas and Eckert [60] and Meyer and Everts [54], free convection effects caused the local Nusselt numbers to decrease near the inlet of the test section and subsequently increase before they became constant.

From the results of Shannon and Depew [61] and Newell and Bergles [55], who conducted experiments using water, free convection effects seemingly increased the thermal entrance length. For hydrodynamically fully developed and thermally developing flow, Newell and Bergles [55] presented the following correlation (with an inaccuracy of ± 30%) to predict the mixed convection thermal entrance length, Lt_{MC}:

$$Lt_{MC} \approx Lt_{FC} + \frac{Re^2}{Gr} \approx 0.05RePrD + \frac{Re^2}{Gr} \tag{5}$$

where Gr is the Grashof number. Newell [39] obtained the term Re^2/Gr from the expressions for the inertia and body force terms to characterise the length required for free convection effects to develop. Although he did not conduct experiments of his own, Eq. (5) compared well with the experimental data of McComas and Eckert [60]. Based on the results of Petukhov and Polyakov [62], Bergles and Simonds [53] reported that the thermal entrance length decreased when free convection effects were significant. Similar observations were also made by Hallman [59], Chen and Ou [63], and Cheng *et al.* [64]. Hong *et al.* [65] investigated laminar flows analytically and experimentally and observed that at a modified Rayleigh number of 10^6, the fully developed Nusselt number, Nu, was approximately 300% greater than that obtained with the constant-property prediction (Nu = 4.36), while the thermal entrance length was only one-tenth of that obtained with the constant-property prediction (Eq. (4)).

Almost no experimental data with low uncertainties that confirm the accuracy of the coefficients of 0.06 (hydrodynamic entrance length) and 0.05 (thermal entrance length) are available in literature. There are only approximately 18 cases available in literature of which only Fargie and Martin [13] quantified the uncertainties of the Reynolds numbers (approximately 6%), and none of them focussed on the thermal entrance length. This is probably because conducting forced convection experiments in tubes where the flow is completely fully developed and the Nusselt number is 4.36 [54] is very challenging. Most of the experimental heat transfer data for pure forced convective laminar flows vary from the theoretical results by 30% or more due to excessive heat losses (very low heat fluxes are required) or free convection effects [60]. Furthermore, no quantitative or experimental information or correlations are available in the literature on the hydrodynamic and thermal entrance lengths in mixed convection conditions. Therefore, the purpose of this study was to develop correlations from experimental data points to determine the thermal and hydrodynamic entrance lengths for simultaneously hydrodynamically and thermally developing

Table 4
Summary of analytical and numerical results of studies that focused on the laminar thermal entrance length in horizontal circular tubes with a constant heat flux boundary condition.

Study	Year	Inlet conditions	Assumptions/comments	Criteria	*Lt/D*	Range
Siegel *et al.* [5]	1958	Fully developed velocity; uniform temperature	Series expansion similar to Graetz solution	$Nu \leq 1.05Nu_{FD}$	$0.0425RePr$	Not specified
Shah [50]	1975	Fully developed velocity; uniform temperature	Graetz solution	$Nu \leq 1.05Nu_{FD}$	$0.043RePr$	Not specified
Pagliarini [23]	1989	Fully developed velocity; uniform temperature	Finite element solution of boundary layer equations	$Nu \leq 1.05Nu_{FD}$	$0.043RePr$	Re = 50, 150, 500, 1 000
Salazar & Campo [51]	1990	Fully developed velocity; uniform temperature	Combined analytical and numerical solution	$Nu \leq 1.05Nu_{FD}$	$0.0434RePr$	Not specified
Nguyen [40]	1992	Fully developed velocity; uniform temperature; isothermal and adiabatic initial conditions	Finite difference solution of boundary layer equations; neglect viscous dissipation	$Nu \leq 1.05Nu_{FD}$	Isothermal initial condition: $-0.000518 + 0.4686/(RePr)$ $0.03263 + 0.3090/(RePr)$ $0.04217 + 0.1309/(RePr)$ Adiabatic initial condition: $0.3120 + 0.2131/(RePr)$ $0.03644 + 0.1901/(RePr)$ $0.04245 + 0.07531/(RePr)$	 $1 < RePr < 5$ $5 < RePr < 20$ $20 < RePr < 1\,000$ $1 < RePr < 5$ $5 < RePr < 20$ $20 < RePr < 1\,000$
Nguyen [24]	1993	Uniform velocity and temperature	Finite difference solution of boundary layer equations	$Nu \leq 1.05Nu_{FD}$	$0.04663 + 0.2836/Re$ $0.05163 + 0.1463/Re$	$1 < Re < 20$ $20 < Re < 1\,000$

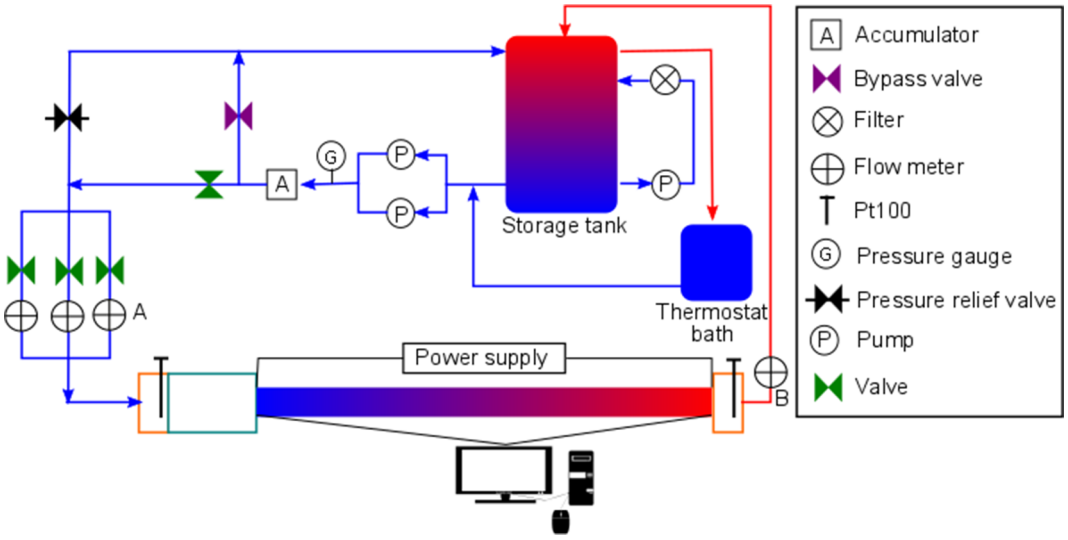

Fig. 2. Schematic of the experimental setup used to conduct the heat transfer and pressure drop measurements. Water was circulated from the storage tank through the test section and back using two pumps. Flowmeter bank A was used to conduct experiments with the 11.5 mm test section and flowmeter B was used for the 4 mm test section.

forced and mixed convective flows. The experimental database used in this study were two orders of magnitude greater than the available experimental data in literature. Furthermore, the uncertainties of the important parameters (such as Reynolds number, Nusselt number and friction factor) as well as the hydrodynamic and thermal entrance length correlations were quantified and in general very low.

2. Experimental setup and test matrix

2.1. Experimental setup

The experimental setup was housed in the Clean Energy Research Group laboratory at the University of Pretoria and is shown schematically in Fig. 2. The experimental setup and test sections that were used have been described in detail in Meyer and Everts [54] and will be discussed only briefly in this paper. The experimental setup consisted of a closed-loop system that circulated the test fluid from a storage tank, through the test section, and back to the storage tank. The storage tank was maintained at a preselected temperature (20 °C) because it was externally connected to a thermostat-controlled bath that cooled the heated fluid.

Three Coriolis mass flow meters with different flow rate capacities were installed in parallel. The mass flow rates were controlled by frequency drives connected to the pump. The required mass flow rate was obtained by increasing or decreasing the pump speed. Downstream of the mass flow meters, the fluid flowed through a flow-calming section (that contained a square-edged inlet) to the test section and mixer, and then back into the storage tank.

Meyer and Everts [54] investigated the effect of different tube diameters (4 mm and 11.5 mm) and heating methods (in-tube heating using a stainless steel tube and heating wire coiled around a copper tube) and concluded that both methods provided accurate heat transfer results. Furthermore, because the Grashof number is proportional to D^3, forced convection conditions could be obtained at higher heat fluxes (and thus lower uncertainties) in a 4 mm test section. Mixed convection conditions with even higher Grashof numbers could be obtained in a 11.5 mm test section [54,57]. Two test sections (internal diameters of 11.5 mm and 4 mm) were therefore used in this study, and are shown schematically in Fig. 3, while the details of the thermocouple stations and pressure taps were provided in Meyer and Everts [54] and Everts

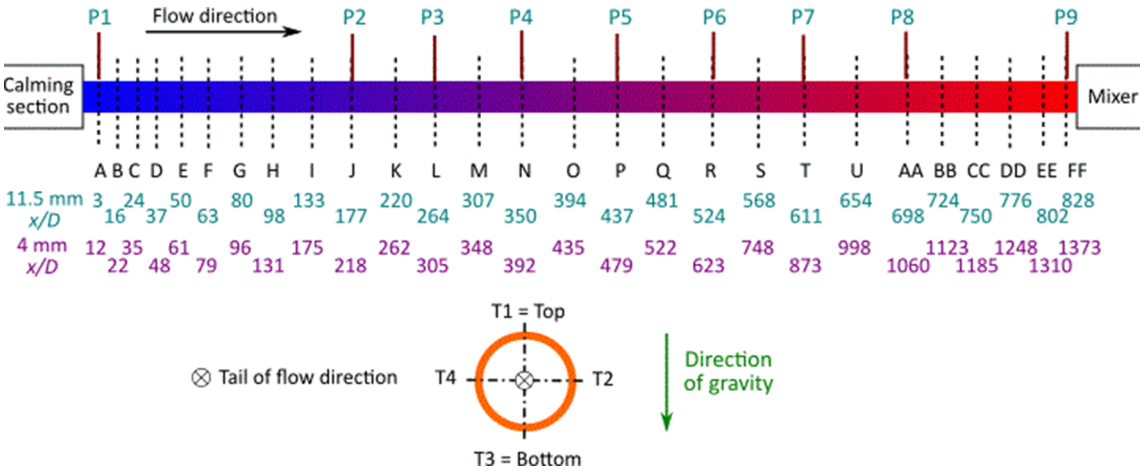

Fig. 3. Schematic of the test sections indicating the 27 thermocouple stations, A to FF, on the 11.5 mm and 4 mm test sections, and the nine pressure taps, P1 to P9, on the 11.5 mm test section. The x/D values of the thermocouple stations of both test sections are also provided. A cross-sectional view of the test section is included to illustrate the position of the four thermocouples spaced around the outer periphery of the tube.

and Meyer [66], respectively.

The 11.5 mm test section was manufactured from a hard-drawn copper tube with an inner diameter, outer diameter, and length of 11.52 mm, 12.7 mm, and 9.81 m, respectively. The 4 mm test section was manufactured from a seamless stainless steel tube with inner and outer diameters of 4 mm and 6 mm, respectively, and a length of 6 m. The average surface roughness (ε) of the 11.5 mm copper and 4 mm stainless steel test sections were measured using a surface roughness tester to be approximately 0.218 μm and 0.138 μm, respectively. Thus, the relative surface roughness (ε/D) were approximately 1.89×10^{-5} and 3.45×10^{-5}, respectively, and for all practical purposes, both tubes were considered smooth. The total lengths of the 11.5 mm and 4 mm test sections provided maximum length-to-inner diameter ratios (x/D) of 828 and 1 373, respectively, while previous investigations by Ghajar and co-workers [67–73] and Meyer and Olivier [74] had maximum values of 400 and 350, respectively. Thus, the test sections were 2–4 times longer than those in previous studies. The longer test sections were required to ensure that fully developed flow was obtained.

T-type thermocouples with a wire diameter of 0.25 mm and an accuracy of 0.1 °C were used to measure the surface temperatures at 27 selected axial positions. The thermocouple stations were spaced close to each other near the inlet of the test section to accurately obtain the temperature profile of the developing flow, and they were spaced further apart on the remainder of the test section where the flow was expected to be fully developed. Four thermocouples (spaced 90° apart around the periphery) were used at each thermocouple station on the 11.5 mm and 4 mm test sections for $x/D < 524$ to investigate possible circumferential temperature distributions caused by free convection effects along the tube length. The remaining thermocouple stations on the 4 mm test section contained thermocouples at the top and bottom of the test section, while the third thermocouple alternated between the left (T4 in Fig. 3) and right (T2 in Fig. 3) side of the test section.

The thermocouples were soldered onto the 11.5 mm copper test section in a 0.3 mm indentation. As the wall thickness of the 4 mm stainless steel tube was 1 mm, the thermocouples were glued into 0.5 mm indentations using a thermal adhesive with a thermal conductivity of 9 W/m.K. The thermocouples of both test sections were calibrated in situ to an accuracy of 0.1 °C by pumping water from the thermostat-controlled bath through the flow-calming section, test section, and mixer, and back into the thermostat-controlled bath. Reference temperatures were obtained using Pt100 probes at the inlet of the flow-calming section, at the outlet of the mixer, and in the thermostat-controlled bath. The temperature of the thermostat-controlled bath was varied between 20 and 60 °C.

Nine pressure taps were fixed to the 11.5 mm test section (Fig. 3) to investigate the hydrodynamic entrance length. The pressure drops were measured between the first pressure tap (P1) and the respective pressure taps (P2 to P8), while the pressure drop of the fully developed region was measured between pressure taps P8 and P9. Differential pressure transducers with interchangeable diaphragms were used to

Table 5
Experimental test matrix generated with water in the 4 mm and 11.5 mm test sections.

Test section	Heat flux [kW/m^2]	Reynolds number range	Number of mass flow rate measurements	Number of temperature measurements*	Number of pressure drop measurements
11.5 mm	0	507–14 968	96	10 464	768
	0.06	303–1 793	28	1 344	–
	1	490–2 659	31	3 379	248
	2	671–2 933	30	3 270	240
	3	723–3 197	25	2 725	200
	6.5	466–2 368	77	4 466	77
	8	469–2 281	61	3 583	61
	9.5	471–2 559	71	4 118	71
4 mm	0.5	913–3 303	32	3 456	–
	1	895–2 027	12	1 296	–
	2	806–2 163	13	1 404	–
	3	790–2 287	13	1 404	–
	4	593–2 460	16	1 728	–
	8	1 143–2 927	8	864	–
Total			513	43 501	1 665

*three or four thermocouples per station.

measure the pressure drops in the axial direction of the test section. DP103 pressure transducers were used to measure the pressure drop across the 1.5 m and 2 m lengths because diaphragms with smaller full scales (and thus higher accuracy) could be used in these pressure transducers. DP15 pressure transducers were used to measure the pressure drop across the other tube lengths. The accuracy of the diaphragms was 0.25% of the full scale. The diaphragms with a full scale smaller than 2.5 kPa were calibrated using a Betz manometer with an accuracy of 2.5 Pa, while the other diaphragms were calibrated using a low-pressure-controlled air manometer with an accuracy of 10 Pa.

Two different heating methods were used in this study because of the availability of equipment. Four constantan wires (connected in parallel) with a diameter of 0.38 mm were coiled around the test section to obtain a constant heat flux boundary condition in the 11.5 mm copper test section. A constant heat flux boundary condition was obtained in the 4 mm stainless steel test section by passing a current through the tube wall. Both test sections were thermally insulated with 120 mm-thick Armaflex insulation with a thermal conductivity of 0.034 W/m.K. The maximum heat loss was estimated by one-dimensional conduction heat transfer calculations to be < 3% in both test sections. Using the criteria of Maranzana *et al.* [75], axial heat conduction was assumed to be negligible in both test sections because the axial heat conduction number was orders of magnitude smaller than 0.01.

2.2. Test matrix

Table 5 summarised the results of the experiments conducted at different mass flow rates and heat fluxes in the two test sections of 11.5 mm and 4 mm. The test matrix consisted of 513 mass flow rate measurements, 43 501 temperature measurements, and 1 665 pressure drop measurements. For a part (Section 5.2) of this study, 512 additional experimental data points obtained by Meyer and Abolarin [76] were used to complement the data in Table 5. While the experiments of Meyer and Abolarin [76] were also conducted using water, a larger tube diameter of 19 mm was used, which led to experimental data with significantly larger Grashof numbers than the data in Table 5.

3. Data reduction

The data reduction method is described in detail in Meyer and Everts [54]; therefore, it will be only briefly discussed in this paper. Because a constant heat flux boundary condition was applied to the test section, the mean fluid temperature, T_m, at a specific tube location, x, was obtained using a linear temperature distribution between the measured inlet, T_i, and measured outlet, T_o, temperatures of the fluid along a tube length, L:

$$T_m = \left(\frac{T_o - T_i}{L}\right)x + T_i \tag{6}$$

The bulk fluid temperature, T_b, along a tube length, $L(x)$, measured from the inlet of the test section, was calculated as follows:

$$T_b = \left(\frac{T_o - T_i}{L}\right)\frac{L(x)}{2} + T_i \tag{7}$$

The properties of water (density, ρ, dynamic viscosity, μ, thermal conductivity, k, specific heat, C_p, Prandtl number, Pr, and thermal expansion coefficient, β) were determined using the thermophysical correlations for liquid water [77] at the bulk fluid temperature for the average properties and at the mean fluid temperature for the local properties at a specific point x , measured from the inlet of the test section.

The Reynolds number, Re, was calculated as follows:

$$Re = \frac{\dot{m}D}{\mu A_c} \tag{8}$$

where $\dot{m}$ is the measured mass flow rate, D is the measured inner-tube diameter, μ is the dynamic viscosity, and A_c is the cross-sectional area of the test section ($A_c = \pi/4D^2$).

The electrical input rate ($\dot{Q}_e = \Delta VI$), which was the product of the voltage drop and current, remained constant, resulting in a constant heat flux. The heat transfer rate to the water, $\dot{Q}_w$, was determined from the measured mass flow rate, measured inlet and outlet temperatures of the water, and the specific heat, which was calculated at the bulk fluid temperature:

$$\dot{Q}_w = \dot{m}C_p(T_o - T_i) \tag{9}$$

The heat transfer rate to the water, $\dot{Q}_w$, was continuously monitored by comparing it to the electrical input rate, $\dot{Q}_e$, which ideally should be equal because the test section is well insulated. The energy balance error, EB, which ideally should be as close as possible to zero, was determined as follows:

$$EB = \left|\frac{\dot{Q}_e - \dot{Q}_w}{\dot{Q}_e}\right| \times 100 = \left|\frac{\Delta VI - \dot{m}C_p(T_o - T_i)}{\Delta VI}\right| \times 100 \tag{10}$$

The average energy balance error of all the experiments conducted was < 3%, which was in positive agreement with the calculations for the estimation of the heat losses to the environment through the insulation material.

The heat flux, $\dot{q}$, on the inside of the tube wall was determined from the heat transfer rate to the water, $\dot{Q}_w$, and the inner surface area, A_s, of the test section along the heated length, L:

$$\dot{q} = \frac{\dot{Q}_w}{A_s} = \frac{\dot{m}C_p(T_o - T_i)}{\pi DL} \tag{11}$$

The average of the four (or three) temperature measurements at a station was used as the average outer surface temperature, $T_{s,o}$, at a specific thermocouple station:

$$T_{s,o} = \frac{T_1 + T_2 + \cdots + T_n}{n} \tag{12}$$

The thermal resistance across the tube wall, R_{tube}, was calculated as:

$$R_{tube} = \frac{ln\left(\frac{D_o}{D}\right)}{2\pi kL} \tag{13}$$

where D_o and D are the measured outer and inner diameters of the tube, respectively. The thermal conductivities of copper and stainless steel are 401 W/m.K and 16.3 W/m.K, respectively. The temperature difference across the tube wall, ΔT, was calculated using Eq. (14) because the thermal resistance and heat input were known:

$$\Delta T = \dot{Q}_w R_{tube} \tag{14}$$

The wall thickness was 0.6 mm, and the thermal resistance in the 11.5 mm test section was calculated to be 4.05×10^{-6} °C/W. Therefore, when the maximum heat input (3 kW/m^2) was applied to the test section, the temperature difference across the tube wall was approximately 0.004 °C. The negligible temperature difference led to the assumption that the temperature on the inner surface of the test section was equal to the temperature measurement on the outer surface of the test section because the temperatures, in general, could only be measured to an accuracy of 0.1 °C.

The thermal resistance in the 4 mm stainless steel test section was calculated to be 3.63×10^{-4} °C/W, which was two orders of magnitude higher than in the 11.5 mm copper test section. The thermocouples in the 4 mm test section were placed in a 0.5 mm deep indentation in the tube wall, and the temperature difference across the remaining 0.5 mm was approximately 0.2 °C when the maximum heat input (8 kW/m^2) was applied to the test section. As this was not negligible, the temperature difference calculated using Eqs. (13) and (14) was subtracted from the measured surface temperatures (Eq. (12)), to obtain the inner surface temperatures, T_s, of the 4 mm test section:

$$T_s = T_{s,o} - \Delta T = T_{s,o} - \dot{Q}_w R_{tube} \tag{15}$$

The average surface temperature of the test section, $\bar{T}_s$, was calculated from all the temperature measurements along the tube length, using the trapezoidal rule:

$$\bar{T}_s = \frac{1}{L(x)} \int_0^{L(x)} T_s(x)dx \tag{16}$$

As the heat flux, $\dot{q}$, surface temperature, T_s, and mean fluid temperature, T_m, were then known, the heat transfer coefficients, h, were determined as follows:

$$h = \frac{\dot{q}}{(T_s - T_m)} \tag{17}$$

The Nusselt numbers, Nu, were determined from the heat transfer coefficients as follows:

$$Nu = \frac{hD}{k} \tag{18}$$

The Grashof numbers, Gr, were determined by:

$$Gr = \frac{g\beta(T_s - T_m)D^3}{\nu^2} \tag{19}$$

where the gravitational acceleration, g, was set to 9.81 m/s^2, and the kinematic viscosity was obtained from the density and dynamic viscosity ($\nu = \mu/\rho$).

The modified Grashof numbers, Gr^*, which are a function of the heat flux rather than the temperature difference, were the product of the Grashof and Nusselt numbers:

$$Gr^* = GrNu = \frac{g\beta\dot{q}D^4}{\nu^2 k} \tag{20}$$

Eqs. (17)–(20) were applicable to local values at a specific axial position along the tube length. The average values along a tube length, $L(x)$, measured from the inlet of the test section, were obtained by using the bulk fluid temperature (Eq. (7)) and average surface temperature (Eq. (16)), instead of the mean fluid temperature (Eq. (6)) and local surface temperature (Eq. (15)).

The average friction factors, f, were calculated from the mass flow rate and pressure drop measurements, ΔP, between two pressure taps that were separated by a length $L(x)$:

$$f = \frac{\Delta P \rho D^5 \pi^2}{8\dot{m}^2 L(x)} \tag{21}$$

In general, the percentage error of a measured or calculated value, M, using the data reduction method above, was determined as % error = $|M_{exp} - M_{cor}|/M_{cor} \times 100$. The average percentage error was regarded as the average of the absolute errors of the data points.

The method suggested by Dunn [78] was used to calculate the uncertainties of the parameters obtained in the data reduction. All uncertainties were calculated within a 95% confidence interval, and the uncertainty analysis details are provided in Everts [79]. The uncertainties of the Reynolds number were approximately 1.5% for all Reynolds numbers. The forced convection Nusselt number uncertainties were < 10%, while the mixed convection uncertainties were < 5% and decreased with increasing heat flux.

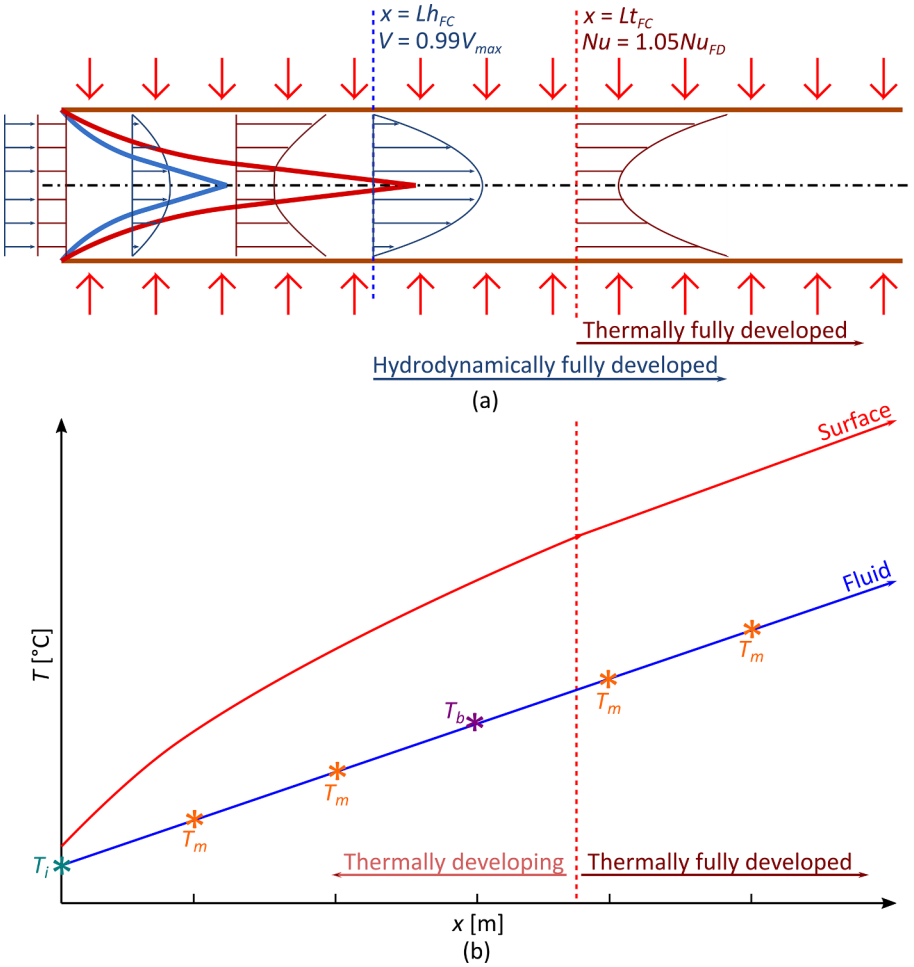

Fig. 4. (a) schematic of the hydrodynamic and thermal boundary layers and (b) surface and fluid temperatures along the tube length of simultaneously hydrodynamically and thermally developing flow through a horizontal tube heated at a constant heat flux.

The uncertainties of the friction factors across the tube lengths $0 < L < 2$ m, $0 < L < 3$ m, and $8 < L < 9.5$ m, were higher (average uncertainty of 13%) than those for the other tube lengths ($0 < L < 4$ m, $0 < L < 5$ m, $0 < L < 6$ m, $0 < L < 7$ m, and $0 < L < 8$ m). This was due to the limitations of the pressure transducer diaphragms because suitable diaphragms with a smaller full-scale were not commercially available. The friction factor uncertainties for the other tube lengths were approximately 10% at the minimum Reynolds number, and decreased to approximately 2% as the Reynolds number increased.

4. Validation

Extensive heat transfer and pressure drop validation experiments were conducted and the details are provided in Meyer and Everts [54] and Everts and Meyer [66], respectively. At a Reynolds number of 941, forced convection conditions in the 11.5 mm test section were obtained at a significantly low heat flux of 60 W/m^2. The average fully developed Nusselt number ($50 < x/D < 827$) was determined to be 4.75, which was within 8.9% of the theoretical value of 4.36 for fully developed forced convection laminar flows. Forced convection conditions at a Reynolds number of 965 in the 4 mm test section were obtained at a heat flux of 1 kW/m^2. The average fully developed Nusselt number ($307 < x/D < 1\,373$) was 4.5, which was within 3.4% of 4.36. The results in both test sections also correlated well with the correlation of Shah and London [3] with an average deviation of 19% in the 11.5 mm test section, while the deviation between $x/D = 567$ and $x/D = 724$ was < 3%. An average deviation of 6% was obtained in the 4 mm test section, while the deviation between $x/D = 307$ and $x/D = 1\,373$ was 1.7%.

The local mixed convection Nusselt numbers in the 11.5 mm and 4 mm test sections were compared with the fully developed flow correlation of Morcos and Bergles [80]. The results correlated well with an average deviation of 6% in the 11.5 mm test section ($37 < x/D < 827$), and an average deviation of 4% in the 4 mm test section ($79 < x/D < 1\,373$). Furthermore, the average mixed convection Nusselt numbers in the 11.5 mm and 4 mm test sections also correlated well with the correlation of Morcos and Bergles [80] with an average deviation of 2 and 4%, respectively.

The developing flow friction factors correlated well with the friction factors predicted by the correlation of Tam *et al.* [72], with an average deviation of 3.3% between Reynolds numbers of 500 and 2 300. The fully developed friction factors correlated well with the Poiseuille flow friction factor of $64/Re$ [81], with an average deviation of 2.5% between Reynolds numbers of 500 and 2 000.

5. Results

Correlations to calculate the thermal and hydrodynamic entrance lengths were developed for both forced and mixed convection conditions. The correlations were developed in terms of the Grashof number (which is a function of the surface-fluid temperature difference) and the modified Grashof number (which is a function of heat flux). Furthermore, for ease of use, sets of correlations were developed in terms of the local fluid properties, fluid properties at the inlet of the tube, and bulk fluid properties inside the tube. Fig. 4 shows a schematic of the temperatures used to calculate the local (at T_m), inlet (at T_i), or bulk (at T_b) fluid properties for simultaneously hydrodynamically and thermally developing flow through a horizontal tube heated at a constant heat flux. This graph is important as it distinguishes between the correct use (and subtle differences) of the temperatures at which the fluid properties should be calculated in the correlations that follow.

The thermal entrance length results are first presented for forced convection conditions and then mixed convection conditions. This is followed by a similar order for the hydrodynamic entrance lengths. The thermal entrance length results are presented first, because the number of temperature measurements were an order of magnitude more than the pressure drop measurements. Furthermore, the temperature measurements could also be measured more accurately. The larger temperature measurement database with lower uncertainties was therefore used as a foundation (in terms of the trends and physics of simultaneously hydrodynamically and thermally developing flow in forced and

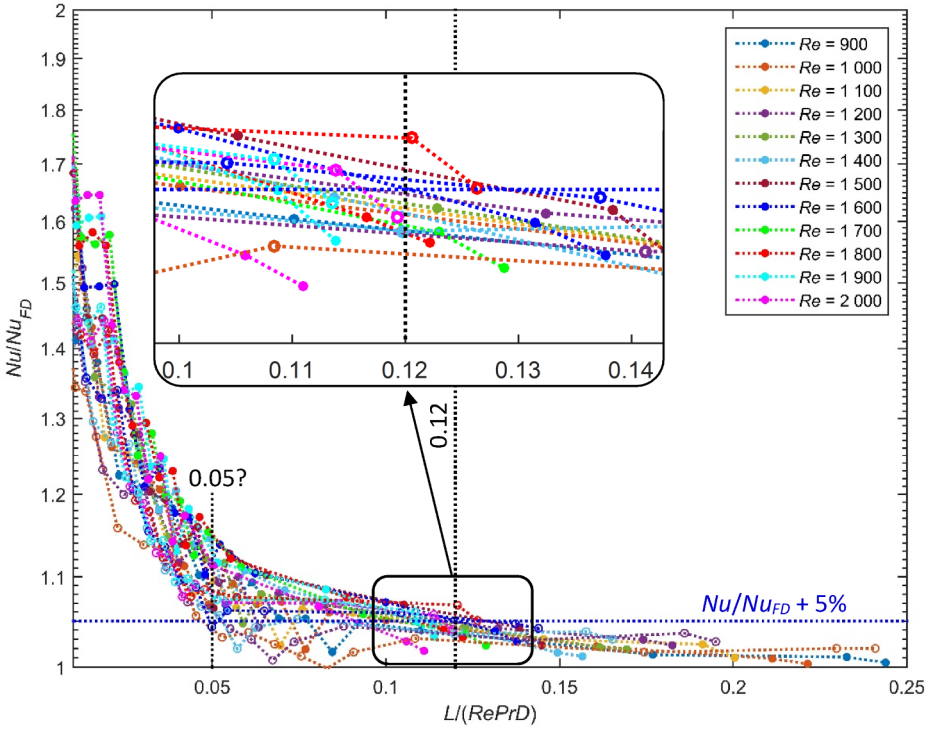

Fig. 5. Comparison of the local laminar Nusselt numbers obtained by Meyer and Everts [54] divided by the fully developed Nusselt number (4.36) as a function of $L/(RePrD)$ for different Reynolds numbers.

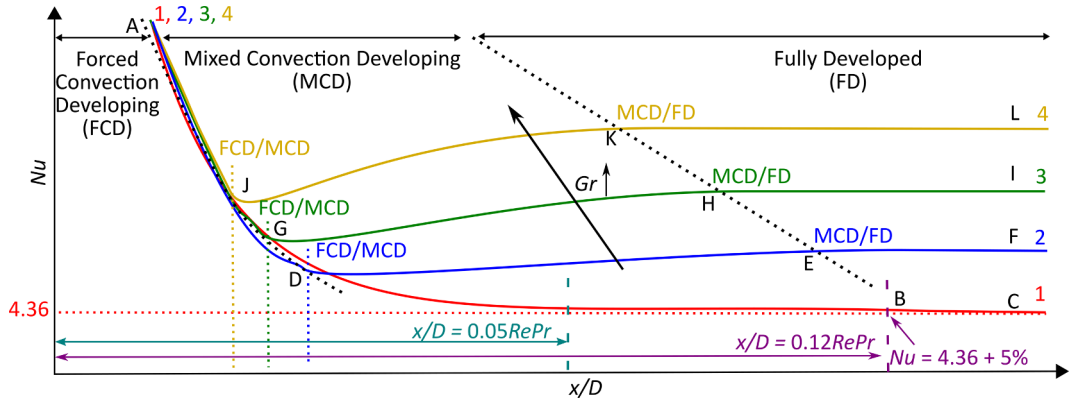

Fig. 6. Schematic of the local Nusselt numbers as a function of axial position for forced and mixed convection conditions. Figure taken from Meyer and Everts [54].

mixed convection conditions) to better interpret and estimate the pressure drop results which are fewer and have higher uncertainties.

5.1. Thermal entrance length: Forced convection

Meyer and Everts [54] observed that Eq. (4) is more suitable for hydrodynamically fully developed and thermally developing flows than for simultaneously hydrodynamically and thermally developing flow. When the flow is simultaneously hydrodynamically and thermally developing, a longer thermal entrance length is required; accordingly, a coefficient of 0.12 was suggested. To verify this, we divided the local Nusselt number data obtained by Meyer and Everts [54] by 4.36 (which is the fully developed laminar Nusselt number for a constant heat flux boundary condition), and plotted them as a function of $L/(RePrD)$, as shown in Fig. 5. Siegel *et al.* [5] considered the flow to be fully developed when the local Nusselt numbers were within 5% of the fully developed Nusselt numbers. Following this consideration, an 5% increase was used as the criterion for fully developed flow conditions and is indicated by the dotted blue line in Fig. 5. Furthermore, the black dotted line represents the suggested coefficient of 0.12 [54].

Similar to the findings of Meyer and Everts [54], Fig. 5 confirms that a coefficient of 0.05 is by far too small and not sufficient when the flow is simultaneously hydrodynamically and thermally developing, because most Nusselt numbers were still above the dotted blue line. The fact that only 5% of the data were below the dotted blue line indicated that the flow was still developing. At the suggested coefficient of 0.12, the dotted black and blue lines indicate that 80% of the data were fully developed. Therefore, Fig. 5 confirms that a coefficient of 0.12 is much more suitable (than 0.05) to determine the thermal entrance length when the flow is simultaneously hydrodynamically and thermally developing:

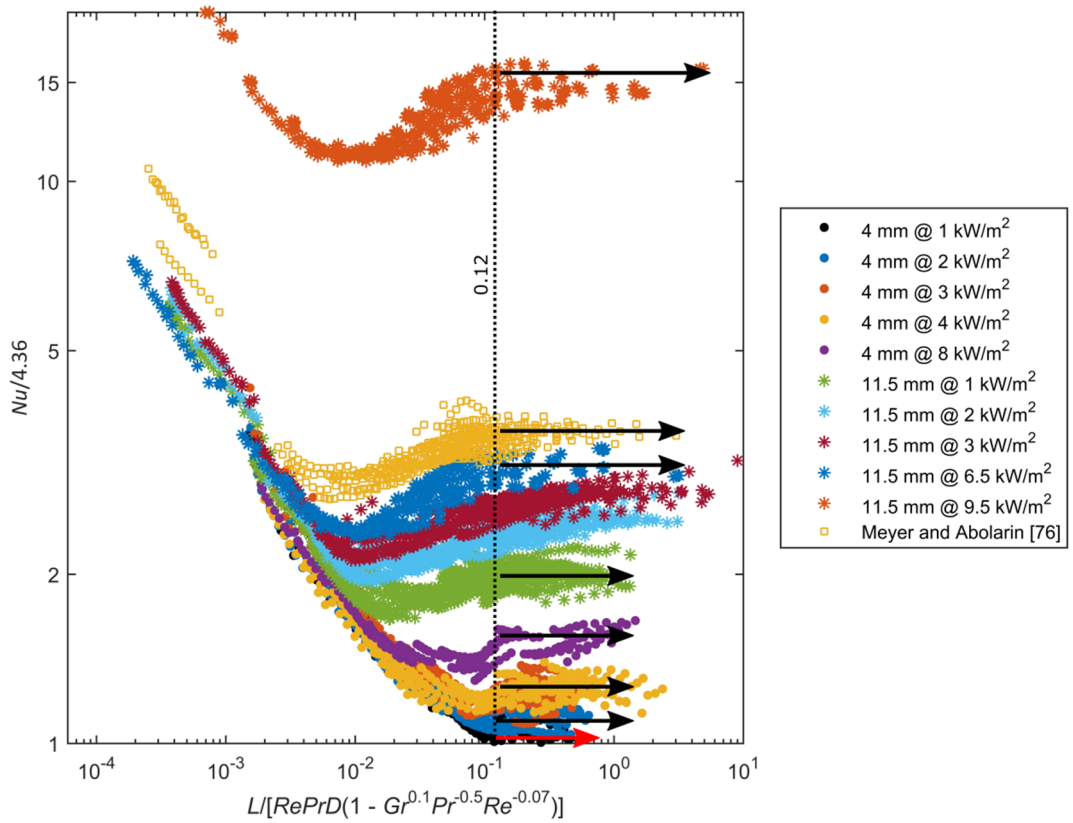

Fig. 7. Comparison of the local laminar Nusselt numbers obtained by Meyer and Everts [54] and Meyer and Abolarin [76] divided by the fully developed Nusselt number (4.36) as a function of $L/[RePrD(1 - Gr^{0.1}Pr^{-0.5}Re^{-0.07})]$ for different heat fluxes and tube diameters.

$$Lt_{FC} = 0.12RePrD \quad (22)$$

The results in Fig. 5 were plotted using the local Reynolds and Prandtl numbers, which might not always be available before experiments and/or during design purposes. Accordingly, the data in Fig. 5 were also expressed in terms of the fluid properties at the inlet of the test section and the bulk fluid properties across a tube length (as schematically indicated in Fig. 4). When either the inlet or the bulk fluid properties were used, only 11% of the data were observed to have a value within 5% for a coefficient of 0.05, but 84% were observed to have a value within 5% when a coefficient of 0.12 was used. Therefore, the forced convection thermal entrance length for simultaneously hydrodynamically and thermally developing flow can also be expressed as either a function of the inlet or bulk fluid properties:

$$Lt_{FC} = 0.12Re_iPr_iD \quad (23)$$

$$Lt_{FC} = 0.12Re_bPr_bD \quad (24)$$

5.2. Thermal entrance length: Mixed convection

Meyer and Everts [54] observed that when mixed convection conditions exist, the trend of the local Nusselt numbers are significantly different from that during forced convection conditions. Fig. 6 contains a schematic of the local Nusselt number trend during forced and mixed convection conditions that were taken from Meyer and Everts [54]. The figure is repeated here for convenience, because a lot of the mixed convection physics will be explained using this figure. The decreasing Nusselt numbers along the tube length in the Forced Convection Developing (FCD) region are due to the increasing thermal boundary layer thickness. As the thermal boundary layer thickness is still very thin near the tube inlet, free convection effects are suppressed. In the Mixed Convection Developing (MCD) region, the thermal boundary layer thickness is sufficient for free convection effects to become significant. Furthermore, free convection effects increase along the tube length due to the increasing thermal boundary layer thickness. As free convection effects assist in diffusing heat from the surface to the centre of the tube, heat transfer inside the tube is enhanced. This explains why the local Nusselt numbers no longer decrease along the tube length (similar to forced convection conditions), but increase in the Mixed Convection Developing region. However, it should be noted that free convection effects disturb the development of the hydrodynamic boundary layer. This explains why the hydrodynamic entrance length in mixed convection conditions (Section 5.4) is longer than in forced convection conditions. Once the flow is fully developed, the thermal boundary layer thickness remains constant along the tube length and therefore free convection effects and the local Nusselt numbers remain constant in the Fully Developed (FD) region.

It is also clear from points E, H, and K in Fig. 6 that the thermal entrance length decreased significantly in mixed convection conditions when free convection effects (thus Grashof number) are increased. This is because free convection effects assist in diffusing the heat from the surface to the centre of the tube and thus also assist in the development of the thermal boundary layer. The result is therefore that the forced convection thermal entrance length correlation became increasingly inaccurate at higher Grashof numbers (or modified Grashof numbers). While the axial position at which the Nusselt numbers became constant decreased with increasing tube diameter (thus increasing the Grashof number), it increased with increasing heat flux (due to the decreasing Prandtl number) for a fixed tube diameter when plotted as a function of $L/(RePrD)$.

To develop a mixed convection thermal entrance length correlation that considers different tube diameters and heat fluxes, and tends to the forced convection thermal entrance length correlation at very low Grashof numbers, we divided the local Nusselt number data obtained by Meyer and Everts [54] and Meyer and Abolarin [76] by 4.36 and plotted them as a function of $L/[RePrD(1 - Gr^mPr^nRe^p)]$, as shown in Fig. 7. The Grashof number was included to account for free convection effects, the Prandtl number to account for different fluids and changes in the fluid properties with temperature, while the Reynolds number was included because it is known from Eq. (4) that the thermal entrance length increase with increasing Reynolds number. Different values for the coefficients m, n, and p, were investigated and it was found that the location at which the values of $Nu/4.36$ became constant corresponded well with $L/[RePrD(1 - Gr^mPr^nRe^p)] = 0.12$ for $m = 0.1$, $n = -0.5$, and

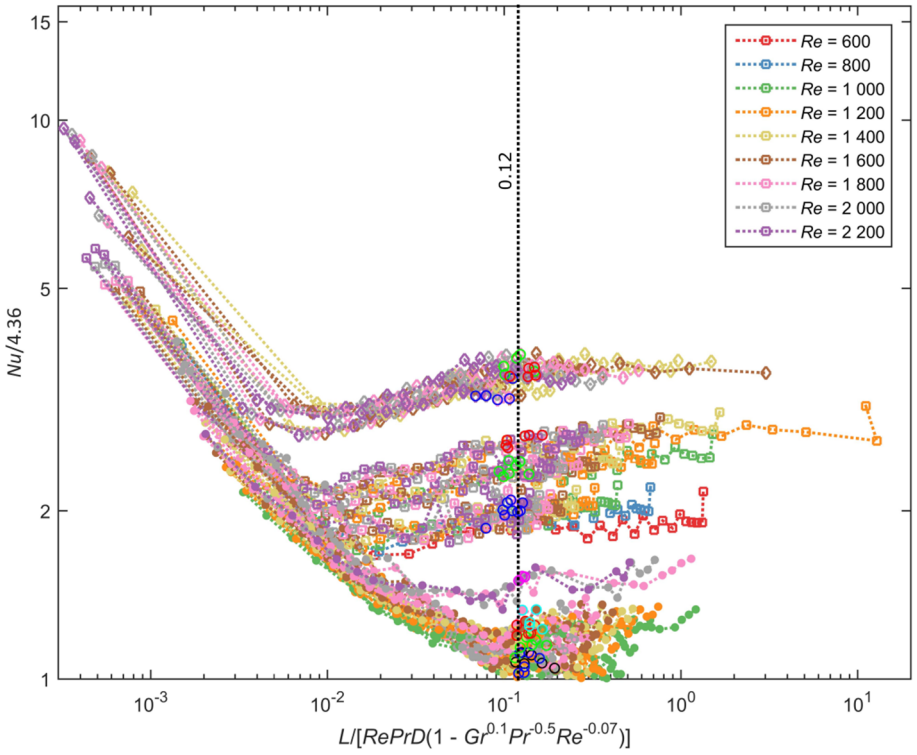

Fig. 8. Comparison of the local laminar Nusselt numbers obtained by Meyer and Everts [54] and Meyer and Abolarin [76] divided by the fully developed Nusselt number (4.36) as a function of $L/[RePrD(1 - Gr^{0.1}Pr^{-0.5}Re^{-0.07})]$ at different Reynolds numbers for different heat fluxes and tube diameters. The empty circles represent the location of fully developed flow for different heat fluxes.

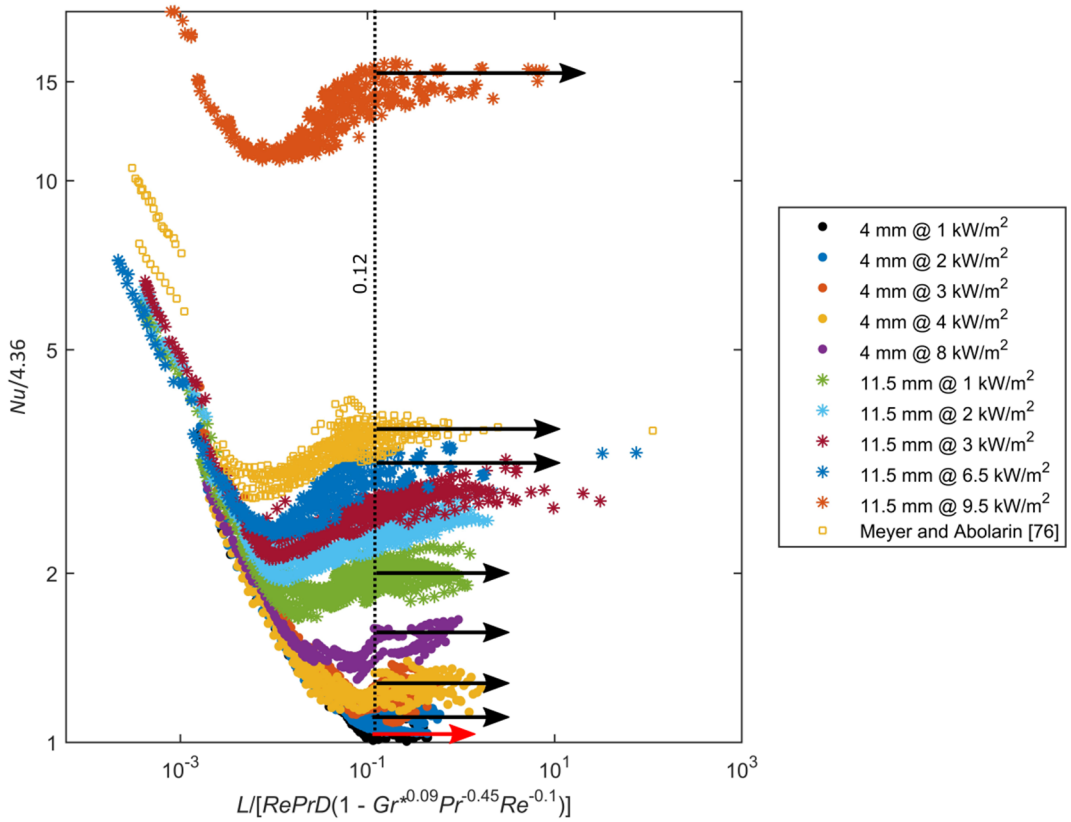

Fig. 9. Comparison of the local laminar Nusselt numbers obtained by Meyer and Everts [54] and Meyer and Abolarin [76] divided by the fully developed Nusselt number (4.36) as a function of $L/[RePrD(1 - Gr^{*0.09}Pr^{-0.45}Re^{-0.1})]$ for different heat fluxes and tube diameters.

p = -0.07. The vertical black dotted line represents a value of 0.12, which corresponds to the coefficient of the forced convection thermal entrance length correlation. The black arrows in Fig. 7 indicate that the Nusselt numbers were constant for $L/[RePrD(1 - Gr^{0.1}Pr^{-0.5}Re^{-0.07})] > 0.12$, which indicated that the flow was fully developed.

The following correlation was obtained to calculate the mixed convection thermal entrance length (and is also expressed in terms of

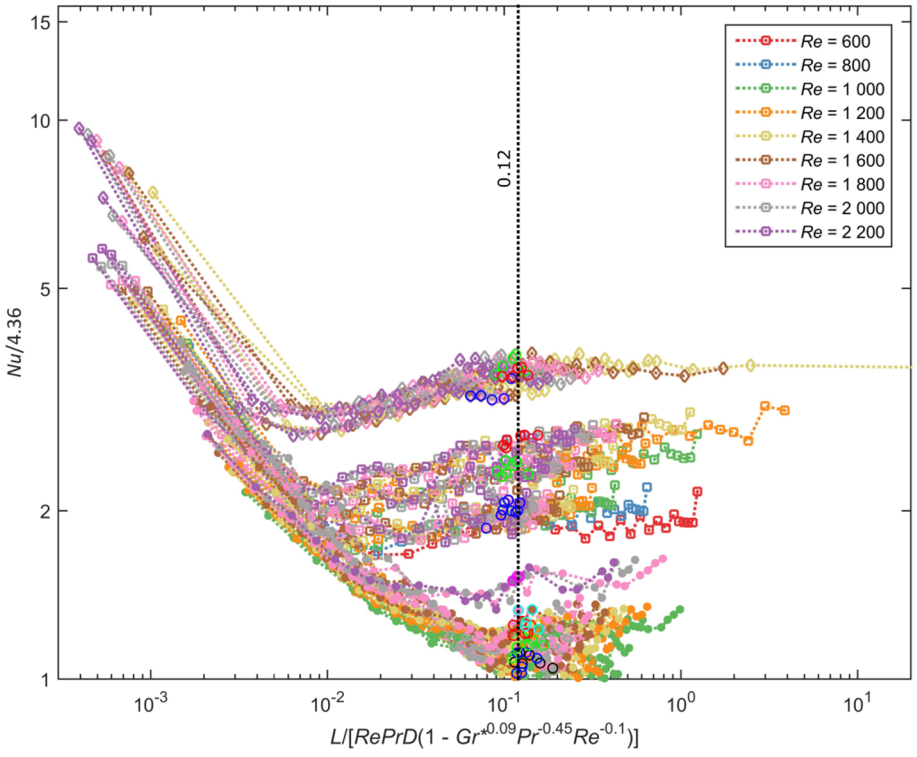

Fig. 10. Comparison of the local laminar Nusselt numbers obtained by Meyer and Everts [54] and Meyer and Abolarin [76] divided by the fully developed Nusselt number (4.36) as a function of $L/[RePrD(1 - Gr^{*0.09}Pr^{-0.45}Re^{-0.1})]$ at different Reynolds numbers for different heat fluxes and tube diameters. The empty circles represent the location of fully developed flow for different heat fluxes.

the forced convection thermal entrance length):

$$Lt_{MC} = \underbrace{0.12RePrD\left(1-\frac{Gr^{0.1}}{Pr^{0.5}Re^{0.07}}\right)}_{\text{Forced convection}} = Lt_{FC}\left(1-\frac{Gr^{0.1}}{Pr^{0.5}Re^{0.07}}\right)_{\text{Mixed convection contribution}} \quad (25)$$

Eq. (25) indicates that the thermal entrance length decreases with increasing Grashof numbers (free convection effects), but increases with increasing Prandtl and Reynolds numbers (similar to the forced convection thermal entrance length). Furthermore, when the Grashof numbers decrease significantly (forced convection conditions exist), Eq. (25) tends to the forced convection thermal entrance length.

To determine the accuracy of Eq. (25), we divided the results obtained by Meyer and Everts [54] and Meyer and Abolarin [76] by 4.36 and plotted them as a function of $L/[RePrD(1 - Gr^{0.1}Pr^{-0.5}Re^{-0.07})]$ for different Reynolds numbers, as shown in Fig. 8. The filled circle and empty square markers represent the data obtained by Meyer and Everts [54] in the 4 mm and 11.5 mm test sections, respectively, while the empty diamond markers represent the data obtained by Meyer and Abolarin [76] in a 19 mm test section. For each Reynolds number, the location of fully developed flow is indicated by an empty circle marker, where the colours of these markers represent different heat fluxes. The flow was considered to be fully developed from the axial position at which the Nusselt numbers became constant.

Fig. 8 indicates that the empty circles (indicating the point where the flow became fully developed) corresponded well to $L/[RePrD(1 - Gr^{0.1}Pr^{-0.5}Re^{-0.07})] = 0.12$ (represented by the vertical black dotted line). Approximately 40% of the circles were within 10%, 76% were within 20%, and the average deviation was 15%.

Similarly, a correlation was also developed in terms of the modified Grashof number because the surface-fluid temperature difference is not always available for constant heat flux applications, while the heat flux most often is. Fig. 9 contains the local Nusselt number data, obtained by Meyer and Everts [54] and Meyer and Abolarin [76], divided by 4.36 as a function of $L/[RePrD(1 - Gr^{*m}Pr^{n}Re^{p})]$. Best results were obtained for $m = 0.09$, $n = -0.45$, and $p = -0.1$, therefore the following correlation was obtained to calculate the mixed convection thermal entrance length (and is also expressed in terms of the forced convection thermal entrance length):

$$Lt_{MC} = 0.12RePrD\left(1-\frac{Gr^{*0.09}}{Pr^{0.45}Re^{0.1}}\right) = Lt_{FC}\left(1-\frac{Gr^{*0.09}}{Pr^{0.45}Re^{0.1}}\right) \quad (26)$$

In Fig. 10, approximately 39% of the circles were within 10%, 76% were within 20%, and the average deviation was 15%.

Note that Eqs. (25) and (26) utilize the local properties along the tube length, which in many cases might not be available. Therefore, similar correlations were also developed in terms of the fluid properties at the inlet of the tube:

$$Lt_{MC} = 0.12Re_iPr_iD\left(1-\frac{Gr_i^{0.11}}{Pr_i^{0.5}Re_i^{0.06}}\right) = Lt_{FC}\left(1-\frac{Gr_i^{0.11}}{Pr_i^{0.5}Re_i^{0.06}}\right) \quad (27)$$

$$Lt_{MC} = 0.12Re_iPr_iD\left(1-\frac{Gr_i^{*0.1}}{Pr_i^{0.5}Re_i^{0.09}}\right) = Lt_{FC}\left(1-\frac{Gr_i^{*0.1}}{Pr_i^{0.5}Re_i^{0.09}}\right) \quad (28)$$

In cases where the inlet conditions are not known, but estimates of the bulk fluid properties are available, Eqs. (29) and (30) can be used:

$$Lt_{MC} = 0.12Re_bPr_bD\left(1-\frac{Gr_b^{0.11}}{Pr_b^{0.5}Re_b^{0.07}}\right) = Lt_{FC}\left(1-\frac{Gr_b^{0.11}}{Pr_b^{0.5}Re_b^{0.07}}\right) \quad (29)$$

$$Lt_{MC} = 0.12Re_bPr_bD\left(1-\frac{Gr_b^{*0.1}}{Pr_b^{0.5}Re_b^{0.08}}\right) = Lt_{FC}\left(1-\frac{Gr_b^{*0.1}}{Pr_b^{0.5}Re_b^{0.08}}\right) \quad (30)$$

Table 6 summarises the mixed convection thermal entrance correlations in terms of the local fluid properties, fluid properties at the inlet of the test section, and bulk fluid properties across the tube length, as well as their ranges. The percentage of the data predicted within 10% and 20% from the experimental data, as well as the average deviation from experimental data, are also summarised in the table.

5.3. Hydrodynamic entrance length: Forced convection

Owing to the relatively large diameter of the 11.5 mm test section, forced convection conditions could only obtained at a very low heat flux of 60 W/m^2, which led to high uncertainties. The isothermal results were therefore used as a guideline for the forced convection hydrodynamic entrance length for simultaneously hydrodynamically and thermally developing flow. The isothermal friction factors were plotted in terms of the Poiseuille number (fRe) as a function of $L/(ReD)$, as shown in Fig. 11, to determine if a coefficient of 0.12 was suitable to calculate the hydrodynamic entrance length (Eq. (1)) for simultaneously hydrodynamically and thermally developing flow. Similar to the fully developed flow criteria used for the local Nusselt numbers in Fig. 5, the dotted blue line indicates the 5% increase which can be used as the criterion for fully developed flow conditions.

The parameter $L/(ReD)$ is similar to $L/(RePrD)$, which was used to obtain the thermal entrance length. The Prandtl number was removed when investigating the hydrodynamic entrance length because Eq. (1) is a function of only the Reynolds number and tube diameter. Note that the pressure drops were not local values, but were the averages of the values measured across tube lengths that varied between 2 m and 8 m. Therefore, when calculating $L/(ReD)$, the bulk Reynolds number corresponding to the centre of the specific tube length, and $L/2$ (which is

Table 6
Mixed convection thermal entrance length correlations and deviation from experimental data.

Properties	Correlation	Eq.	± 10% [%]	± 20% [%]	Average [%]
Local temperatures	$Lt_{MC} = 0.12RePrD\left(1-\frac{Gr^{0.1}}{Pr^{0.5}Re^{0.07}}\right)$	(25)	40	76	15
	$Lt_{MC} = 0.12RePrD\left(1-\frac{Gr^{*0.09}}{Pr^{0.45}Re^{0.1}}\right)$	(26)	50	82	14
Inlet temperature	$Lt_{MC} = 0.12Re_iPr_iD\left(1-\frac{Gr_i^{0.11}}{Pr_i^{0.5}Re_i^{0.06}}\right)$	(27)	51	81	14
	$Lt_{MC} = 0.12Re_iPr_iD\left(1-\frac{Gr_i^{*0.1}}{Pr_i^{0.5}Re_i^{0.09}}\right)$	(28)	53	85	12
Bulk temperature	$Lt_{MC} = 0.12Re_bPr_bD\left(1-\frac{Gr_b^{0.11}}{Pr_b^{0.5}Re_b^{0.07}}\right)$	(29)	39	65	19
	$Lt_{MC} = 0.12Re_bPr_bD\left(1-\frac{Gr_b^{*0.1}}{Pr_b^{0.5}Re_b^{0.08}}\right)$	(30)	41	71	16
	Range $467 < Re < 3\,198$, $2.9 < Pr < 7.6$, $30.6 < Gr < 4.51 \times 10^5$, $541 < Gr^* < 4.01 \times 10^6$, $4\text{ mm} < D < 19\text{ mm}$				

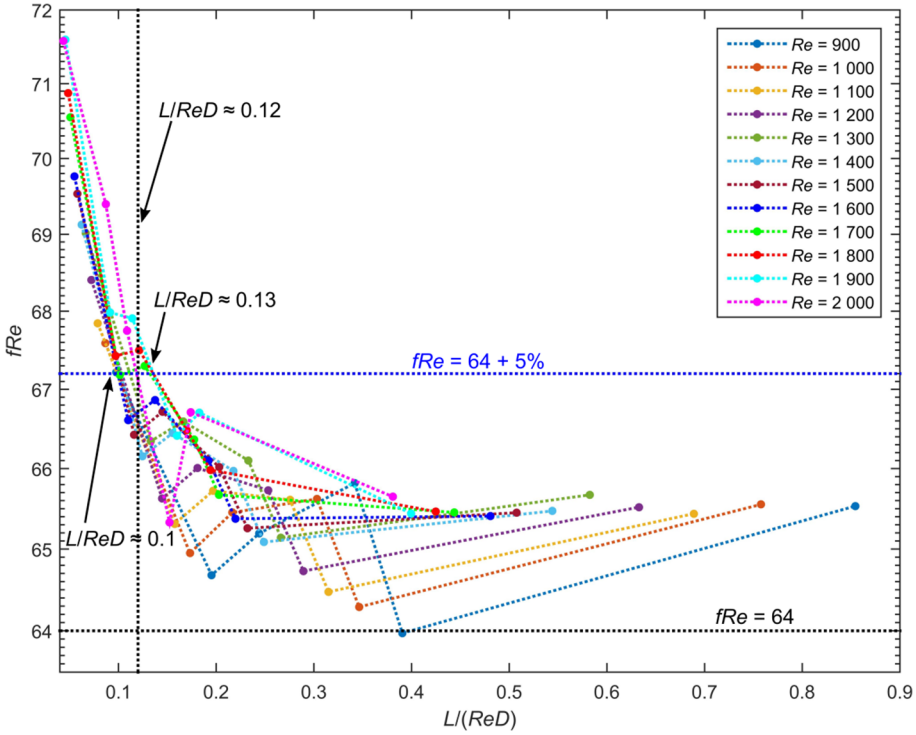

Fig. 11. Comparison of isothermal friction factors obtained by Everts and Meyer [66] multiplied by the Reynolds number (*fRe*) as a function of *L/(ReD)* for different Reynolds numbers. (For interpretation of the references to colour in this figure legend, the reader is referred to the web version of this article.)

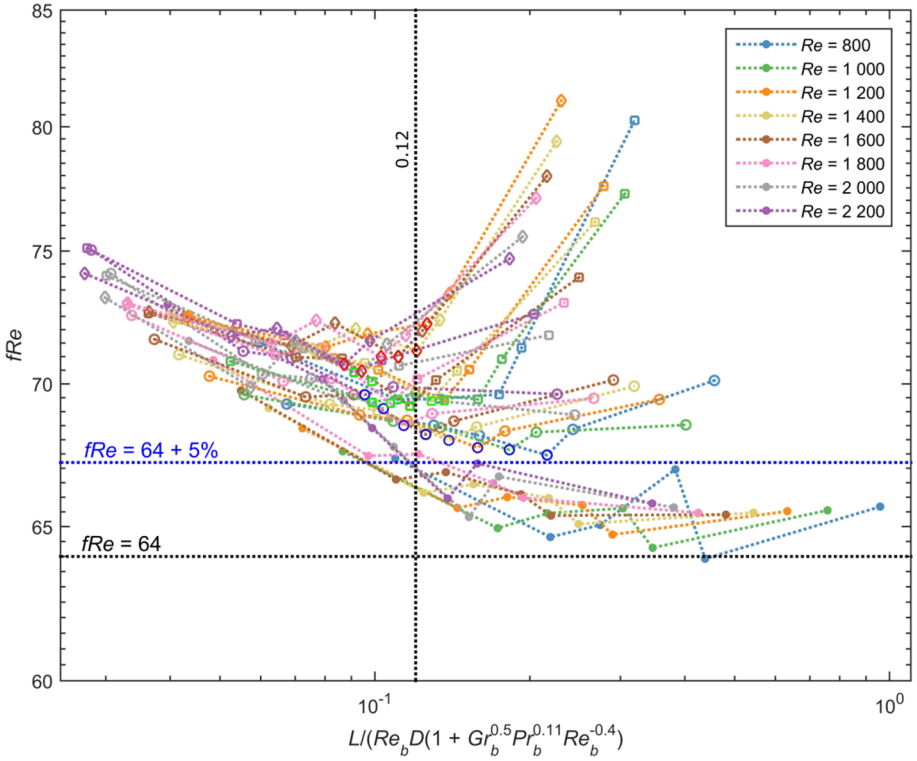

Fig. 12. Comparison of the isothermal and diabatic friction factors obtained by Everts and Meyer [66] multiplied by the Reynolds number (*fRe*) as a function of $L/[ReD(1 + Gr_b^{0.5}Pr_b^{0.11}Re_b^{-0.4})]$ for different Reynolds numbers. The solid markers represent the isothermal data, while the empty circle, square, and diamond markers represent the diabatic data at heat fluxes of 1, 2, and 3 kW/m^2, respectively. The empty blue, green and red circles represent the location of fully developed flow for heat fluxes of 1, 2, and 3 kW/m^2. (For interpretation of the references to colour in this figure legend, the reader is referred to the web version of this article.)

the centre of that tube length) were used.

Fig. 11 indicates that the results of the different tube lengths crossed the 5% line at $0.1 < L/(ReD) < 0.13$, which is consistent with a coefficient of 0.12 for the thermal entrance length. The fact that the same coefficient of 0.12 can be used for both the thermal and the hydrodynamic entrance lengths is very convenient and most probably due to the relationship/analogy that exist between heat transfer and pressure drop [66]. Although this coefficient of 0.12 was obtained from the isothermal friction factors, it is expected to be also valid for forced convection conditions when the flow is simultaneously hydrodynamically and thermally developing. In the laminar flow regime, the pressure drops are very small; therefore, the uncertainties of the friction factors were larger (2.5–16%) than in the turbulent flow regime (< 4%) [66]. Considering the uncertainty of the pressure drop measurements,

we can conclude that a coefficient of 0.12 should also be used when calculating the hydrodynamic entrance length for simultaneously hydrodynamically and thermally developing flow:

$$Lh_{FC} = 0.12ReD \tag{31}$$

5.4. Hydrodynamic entrance length: Mixed convection

Everts and Meyer [66] investigated the relationship between heat transfer and pressure drop in the laminar, transitional, quasi-turbulent, and turbulent flow regimes. They observed that a direct relationship existed in all four flow regimes and the boundaries between the flow regimes were also the same for the heat transfer and pressure drop results. Because the thermal entrance length was significantly affected by free convection effects, the mixed convection hydrodynamic entrance length can be expected to be different from Eq. (1).

The diabatic friction factors obtained by Everts and Meyer [66] were plotted in terms of the Poiseuille number (fRe) as a function of $L/[Re_bD(1 + Gr_b^mPr_b^nRe_b^p)]$, as shown in Fig. 12, to determine the mixed convection hydrodynamic entrance length. Similar to the mixed convection thermal entrance length, the Grashof number was included to account for free convection effects, the Prandtl number to account for different fluids and changes in the fluid properties with temperature, while the Reynolds number was included because it is known from Eq. (1) that the hydrodynamic entrance length increase with increasing Reynolds number. Similar to the forced convection hydrodynamic entrance length, $L/2$ (which is the centre of that tube length) was used.

Unlike the isothermal results in Fig. 11, the diabatic friction factors did not decrease and become constant when the flow was fully developed. Because the tube was heated at different constant heat fluxes, the fluid temperature increased along the tube length, which caused the density and viscosity of the fluid to decrease, and the pressure drop and friction factors to decrease compared with the isothermal results. The local friction factors therefore continued to decrease along the tube length and did not experience regions of increasing or constant friction factors similar to the local mixed convection Nusselt numbers in the Mixed Convection Developing and Fully Developed regions (Fig. 6). However, the Reynolds numbers along the tube length increased because they are inversely proportional to the viscosity, which decreased. An initial decrease in the Poiseuille number was observed along the tube length as the flow developed because the decrease in friction factors (due to entrance effects) dominated the increase in Reynolds number (due to heating). However, when the flow was fully developed, the friction factors continued to decrease (due to free convection effects) but were dominated by the increasing Reynolds numbers (due to free convection effects); therefore, the Poiseuille numbers began to increase. Thus, the flow was considered to be hydrodynamically fully developed from the axial position at which the Poiseuille numbers began to increase.

In Fig. 12, the solid markers represent the isothermal data, while the empty circle, square, and diamond markers represent the diabatic data at heat fluxes of 1, 2, and 3 kW/m^2, respectively. Different values for the coefficients m, n, and p, were investigated and it was found that the location at which the Poiseuille numbers began to increase corresponded well with $L/[Re_bD(1 + Gr_b^mPr_b^nRe_b^p)] = 0.12$ for $m = 0.05$, $n = 0.11$, and $p = -0.4$. The empty blue, green, and red circles in Fig. 12 represent the locations at which the flow became fully developed for heat fluxes of 1, 2, and 3 kW/m^2, respectively.

The black dotted line in Fig. 12 corresponds to $L/[Re_bD(1 + Gr_b^{0.5}Pr_b^{0.11}Re_b^{-0.4})] = 0.12$, which ensures that, similar to the thermal entrance length correlations, the mixed convection hydrodynamic entrance length correlation tends to the forced convection correlation (Eq. (31)) when free convection effects are negligible ($Gr \rightarrow 0$). The following correlation was obtained to calculate the mixed convection hydrodynamic entrance length (and is also expressed in terms of the forced convection hydrodynamic entrance length):

$$Lh_{MC} = \underbrace{0.12Re_bD\left(1+\frac{Gr_b^{0.5}Pr_b^{0.11}}{Re_b^{0.4}}\right)}_{\text{Forced convection}} = \underbrace{Lh_{FC}\left(1+\frac{Gr_b^{0.5}Pr_b^{0.11}}{Re_b^{0.4}}\right)}_{\text{Mixed convection contribution}} \tag{32}$$

An interesting observation from Eq. (32) is that, although free

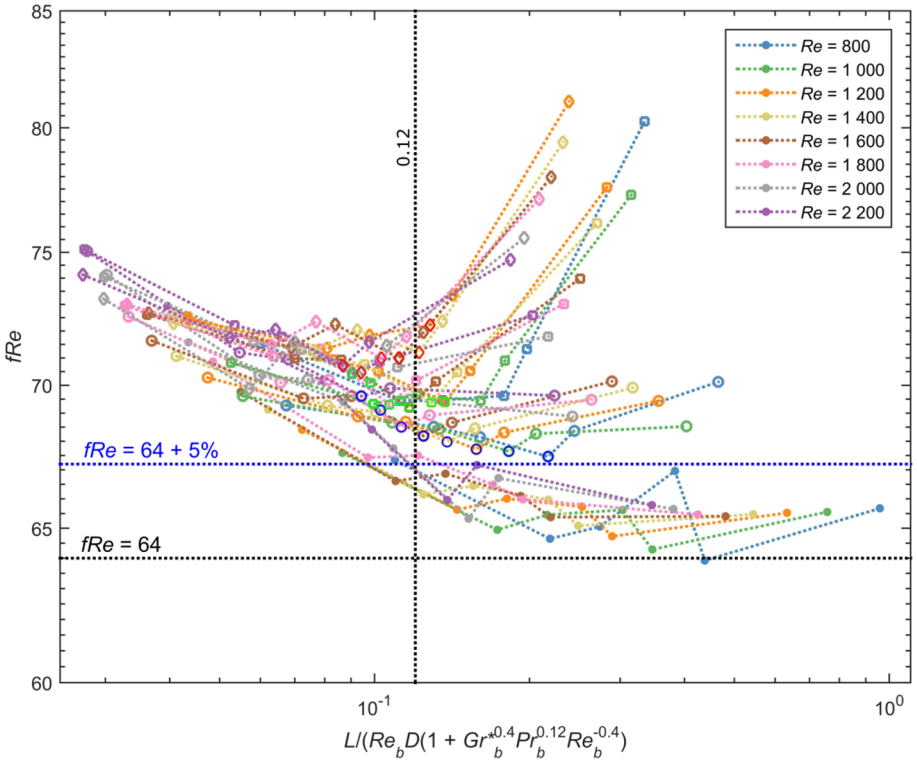

Fig. 13. Comparison of the isothermal and diabatic friction factors obtained by Everts and Meyer [66] multiplied by the Reynolds number (fRe) as a function of $L/[Re_bD(1 + Gr^{*0.4}_bPr_b^{0.12}Re_b^{-0.4})]$ for different Reynolds numbers. The solid markers represent the isothermal data, while the empty circle, square, and diamond markers represent the diabatic data at heat fluxes of 1, 2, and 3 kW/m^2, respectively. The empty blue, green and red circles represent the location of fully developed flow for heat fluxes of 1, 2, and 3 kW/m^2. (For interpretation of the references to colour in this figure legend, the reader is referred to the web version of this article.)

Table 7
Mixed convection hydrodynamic entrance length correlations and deviation from experimental data.

Properties	Correlation	Eq.	± 10% [%]	± 20% [%]	Average [%]
Bulk temperature	$Lh_{MC} = 0.12 Re_b D\left(1 + \frac{Gr_b^{0.5} Pr_b^{0.1}}{Re_b^{0.4}}\right)$	(31)	40	72	18
	$Lh_{MC} = 0.12 Re_b D\left(1 + \frac{Gr_b^{*0.4} Pr_b^{0.12}}{Re_b^{0.4}}\right)$	(32)	40	72	18
Inlet temperature	$Lh_{MC} = 0.12 Re_i D\left(1 + \frac{Gr_i^{0.6} Pr_i^{0.1}}{Re_i^{0.4}}\right)$	(33)	36	73	18
	$Lh_{MC} = 0.12 Re_i D\left(1 + \frac{Gr_i^{*0.45} Pr_i^{0.1}}{Re_i^{0.4}}\right)$	(34)	36	63	19
	Range $512 < Re < 3\,083$, $3.3 < Pr < 6.8$, $6.7 \times 10^3 < Gr < 1.0 \times 10^5$, $6.1 \times 10^4 < Gr^* < 1.4 \times 10^6$, $D = 11.5$ mm				

convection effects decrease the thermal entrance length, they disturb the development of the hydrodynamic boundary layers and cause the hydrodynamic entrance length to be greater than that in forced convection conditions. The empty circles in Fig. 12 indicate that Eq. (32) performed reasonably well and could predict 40% of the data within 10%, 72% of the data within 20%, and the average deviation as 18%. Although these deviations are much larger than for the thermal entrance length correlations, the uncertainties of the pressure drop measurements were higher (an average deviation of 13%) than for the temperature measurements (maximum deviation of 5%). Therefore, we can conclude that Eq. (32) performed well within the uncertainties.

Similarly, a mixed convection hydrodynamic entrance length correlation was also developed in terms of the modified Grashof number. Fig. 13 depicts the diabatic friction factors obtained by Everts and Meyer [66] in terms of the Poiseuille number (fRe) as a function of $L/[Re_b D(1 + Gr^*_b{}^{0.4} Pr_b^{0.12} Re_b^{-0.4})]$.

The following correlation was obtained to calculate the mixed convection hydrodynamic entrance length (and is also expressed in terms of the forced convection hydrodynamic entrance length):

$$Lh_{MC} = 0.12 Re_b D\left(1 + \frac{Gr_b^{*0.4} Pr_b^{0.12}}{Re_b^{0.4}}\right) = Lh_{FC}\left(1 + \frac{Gr_b^{*0.4} Pr_b^{0.12}}{Re_b^{0.4}}\right) \quad (33)$$

The empty circles in Fig. 13 indicate that Eq. (33) performed reasonably well and could predict 40% of the data within 10%, 72% of the data within 20%, and the average deviation as 18.4%.

Because Eqs. (32) and (33) are functions of the bulk fluid properties, similar correlations were also developed in terms of the properties at the inlet of the test section:

$$Lh_{MC} = 0.12 Re_i D\left(1 + \frac{Gr_i^{0.6} Pr_i^{0.1}}{Re_i^{0.4}}\right) = Lh_{FC}\left(1 + \frac{Gr_i^{0.6} Pr_i^{0.1}}{Re_i^{0.4}}\right) \quad (34)$$

$$Lh_{MC} = 0.12 Re_i D\left(1 + \frac{Gr_i^{*0.45} Pr_i^{0.1}}{Re_i^{0.4}}\right) = Lh_{FC}\left(1 + \frac{Gr_i^{*0.45} Pr_i^{0.1}}{Re_i^{0.4}}\right) \quad (35)$$

Table 7 summarises the mixed convection hydrodynamic entrance length correlations in terms of the bulk properties and properties at the inlet of the test section, as well as their ranges. The percentage of the data predicted within 10% and 20% from the experimental data, as well as the average deviation from experimental data, are also summarised in the table.

5.5. Uncertainties of entrance length correlations

By using the method suggested by Dunn [78], the uncertainties of the hydrodynamic and thermal entrance length correlations were calculated within a 95% confidence interval. The average uncertainties of the hydrodynamic and thermal entrance length correlations were approximately 2% and 5%, respectively. The challenge with these uncertainties are that they are very low in comparison with the uncertainties of the friction factors and Nusselt numbers. There are two main reasons for this: (1) The uncertainties of the correlations are based on the Reynolds number, Prandtl number, Grashof number, and tube diameter, which are generally low (except for the Grashof number) compared with the uncertainties of the friction factors and Nusselt numbers. (2) The uncertainty calculations do not take into account the visual observations/decisions/estimates that were made to determine the coefficient of 0.12. Other scholars might differ on this value.

6. Conclusions

The purpose of this study was to experimentally investigate the hydrodynamic and thermal entrance lengths for laminar flow in smooth horizontal tubes heated at a constant heat flux. Simultaneously hydrodynamically and thermally developing flow was investigated for both forced and mixed convection conditions. Two smooth circular test sections with inner diameters of 4 mm and 11.5 mm were used, and the maximum length-to-diameter ratios were 1 373 and 872, respectively. Heat transfer and pressure drop measurements were taken at Reynolds numbers between 460 and 3 200 at different heat fluxes. A total of 513 mass flow rate measurements, 43 501 temperature measurements, and 1 665 pressure drop measurements were conducted. Water was used as the test fluid and the Prandtl number ranged between 3 and 8.

When the flow was simultaneously hydrodynamically and thermally developing through a horizontal tube heated at a constant heat flux, a longer thermal entrance length was required compared with that required for a flow that was hydrodynamically fully developed before the thermal boundary layers began to develop. Therefore, a coefficient of 0.12 was proposed instead of 0.05, which is recommended in most heat transfer textbooks. This coefficient of 0.12 was observed to be sufficient when the local, inlet, or bulk fluid properties were used in the forced convection thermal entrance length correlation.

In a mixed convective flow, the free convection effects were observed to assist the flow in becoming thermally fully developed; therefore, the thermal entrance length decreased significantly. Correlations were developed in terms of the Grashof number (which is a function of the surface-fluid temperature difference) and the modified Grashof number (which is a function of heat flux) to account for free convection effects. The form of the correlations is such that as the Grashof number (or modified Grashof number) tended to zero (forced convection conditions), the correlations tended to the forced convection thermal entrance length correlations. Thus, three sets of correlations were developed to calculate the mixed convection thermal entrance lengths in terms of the local, inlet, and bulk fluid properties. All six correlations performed well and the average deviation between the mixed convection thermal entrance lengths predicted using the correlations and that obtained from experimental results varied between 12 and 19%. In general, the correlations in terms of the inlet fluid properties had the best performance and could predict > 80% of the data within 20%.

In a simultaneously hydrodynamically and thermally developing

flow, the development of the thermal boundary layers also led to a longer hydrodynamic entrance length. Therefore, similar to the forced convection thermal entrance length correlation, a coefficient of 0.12 (and not 0.06 as recommended in most fluid mechanics papers and textbooks) was proposed.

Similar to the mixed convective thermal entrance length, correlations for the mixed convective hydrodynamic entrance length in terms of both the Grashof and modified Grashof numbers were developed and also tended to the forced convection correlation when free convection effects became negligible. However, it is important to note that although free convection effects caused the mixed convective thermal entrance length to decrease, the mixed convective hydrodynamic entrance length increased compared with forced convection conditions. Both sets of mixed convective hydrodynamic entrance length correlations (in terms of the bulk and inlet fluid properties) performed well and could predict 70% of the data within 20%, and the average deviation from the experimental data was approximately 18%.

The coefficient of 0.12 that is valid for both the hydrodynamic and thermal forced convective entrance length, and the mixed convection correlations that tend to the forced convection ones when free convection effects are negligible, are very elegant results of this study. The uncertainties of the correlations were also determined, but was found to be less than that of the Nusselt numbers and friction factors, as the uncertainty related to the visual observations/decisions/estimates of the coefficient (0.12) was not taken into account.

In this paper, we presented the first large database of experimental data with uncertainties of hydrodynamic and thermal entrance lengths for simultaneously hydrodynamically and thermally developing forced and mixed convective laminar flow in horizontal tubes heated at a constant heat flux. Nevertheless, more experimental work is required. This should specifically entail more accurate pressure drop measurements, a range of test fluids (to ensure a wider Prandtl number range), and various inlet geometries (re-entrant, square-edged, and bellmouth). Furthermore, the hydrodynamic and thermal entrance lengths for simultaneously hydrodynamically and thermally developing forced and mixed convective laminar flow in horizontal tubes at a constant surface temperature should be developed.

CRediT authorship contribution statement

Marilize Everts: Conceptualization, Data curation, Formal analysis, Funding acquisition, Investigation, Methodology, Validation, Writing - original draft. **Josua P. Meyer:** Conceptualization, Funding acquisition, Resources, Supervision, Writing - review & editing.

Declaration of Competing Interest

The authors declared that there is no conflict of interest.

Acknowledgements

The funding obtained in South Africa from the National Research Foundation (Grant Number: 116623), Department of Science and Innovation (DSI), and University of Pretoria is acknowledged and duly appreciated.

References

[1] R.K. Shah, A correlation for laminar hydrodynamic entry length solutions for circular and noncircular ducts, J. Fluids Eng. 100 (June) (1978) 177–179.
[2] A.K. Mohanty, S.B.L. Asthana, Laminar flow in the entrance region of a smooth pipe, J. Fluid Mech. 90 (3) (1979) 433–447.
[3] R.K. Shah, A.L. London, Laminar Flow Forced Convection in Ducts, Academic Press, New York, 1978.
[4] J.H.I. Lienhard, J.H.V. Lienhard, A Heat Transfer Textbook, 3rd ed., Phlogiston Press, Cambridge, 2008.
[5] R. Siegel, E.M. Sparrow, T.M. Hallman, Steady laminar heat transfer in a circular tube with a prescribed wall heat flux, Appl. Sci. Res. 7 (1958).
[6] J.R. Bodoia, J.F. Osterle, Finite difference analysis of plane Poiseuille and Couette flow developments, Appl. Sci. Res. 10 (1) (1961) 265.
[7] W.D. Campbell, J.C. Slattery, Flow in the Entrance of a Tube, J. Basic Eng. 85 (1) (1963) 41–45.
[8] J. Boussinesq, Sur la maniere don't les vitesses, dans un tube cylindrique de section circulaire, evase a son entrée, se distribuent depuis entrée jusqu'aux endroits ou se trouve etabli un regime uniforme, Comptes Rendus 113 (1891) 49–51.
[9] H.L. Langhaar, Steady flow in the transition length of a straight tube, J. Appl. Mech. 9 (1942) A-55-A-58.
[10] L. Schiller, Die Entwicklung der laminaren Geschwindigkeitsverteilung und ihre Bedeutung für Zähigkeitsmessungen., (Mit einem Anhang über den Druckverlust turbulenter Strömung beim Eintritt in ein Rohr.), ZAMM – Journal of Applied Mathematics and Mechanics / Zeitschrift für Angewandte Mathematik und Mechanik 2 (2) (1922) 96–106.
[11] R. Siegel, The effect of heating on boundary layer transition for liquid flow in a tube, PhD thesis Massachusetts Institute of Technology, Boston, 1953.
[12] S.T. McComas, Hydrodynamic entrance lengths for ducts of arbitrary cross section, J. Fluids Eng. Trans. ASME 89 (4) (1967) 847–850.
[13] D. Fargie, B.W. Martin, Developing Laminar Flow in a Pipe of Circular Cross-Section, Proceedings of the Royal Society of London. Series A, Mathematical and Physical Sciences, 321(1547) (1971) 461-476.
[14] R.Y. Chen, Flow in the entrance region at low Reynolds numbers, J Fluids Eng Trans ASME 95 (1) (1973) 153–158.
[15] Z. Matras, J. Stachura, Laminar flow of Newtonian fluid in the entrance region of a circular pipe, Archiwum Hydrotechniki 28 (2) (1981) 189–203.
[16] J.P. Du Plessis, M.R. Collins, A new definition for laminar flow entrance lengths of straight ducts, R&D J. – SAIMechE 8 (September) (1992) 11–16.
[17] S.W. Churchill, R. Usagi, A general expression for the correlation of rates of transfer and other phenomena, AIChE J. 18 (6) (1972) 1121–1128.
[18] R.W. Hornbeck, Laminar flow in the entrance region of a pipe, Appl. Sci. Res. 13 (1) (1964) 224–232.
[19] E.B. Christiansen, H.E. Lemmon, Entrance region flow, AIChE J. 11 (6) (1965) 995–999.
[20] J.S. Vrentas, J.L. Duda, K.G. Bargeron, Effect of axial diffusion of vorticity on flow development in circular conduits: Part I, Numerical Solut. AIChE J. 12 (5) (1966) 837–844.
[21] M. Friedmann, J. Gillis, N. Liron, Laminar flow in a pipe at low and moderate Reynolds numbers, Appl. Sci. Res. 19 (1) (1968) 426–438.
[22] B. Atkinson, M.P. Brocklebank, C.C.H. Card, J.M. Smith, Low Reynolds number developing flows, AIChE J. 15 (4) (1969) 548–553.
[23] G. Pagliarini, Steady laminar heat transfer in the entry region of circular tubes with axial diffusion of heat and momentum, Int. J. Heat Mass Transf. 32 (6) (1989) 1037–1052.
[24] T.V. Nguyen, Incremental heat transfer number in the entry region of circular tubes, Int. J. Heat Mass Transf. 36 (14) (1993) 3659–3662.
[25] F. Durst, S. Ray, B. Ünsal, O.A. Bayoumi, The development lengths of laminar pipe and channel flows, J Fluids Eng Trans ASME 127 (6) (2005) 1154–1160.
[26] Y. Joshi, B.R. Vinoth, Entry lengths of laminar pipe and channel flows, J Fluids Eng Trans ASME 140 (6) (2018).
[27] O.K.G. Tietjens, Applied Hydro- and Aeromechanics : Based on Lectures of L, Prandtl, McGraw-Hill, New York, 1934.
[28] M.P. Brocklebank, J.M. Smith, Laminar velocity profile development in straight pipes of circular cross section, Rheol. Acta 7 (3) (1968) 286–289.
[29] F.M. White, Fluid Mechanics, 8th ed., McGraw-Hill, Singapore, 2016.
[30] R.A.-C.E. American, Society of Heating Inc, 2017 ASHRAE Handbook - Fundamentals (SI Edition), American Society of Heating, Refrigerating and Air-Conditioning, Engineers, Inc. (ASHRAE), 2017.
[31] M.C. Potter, D.C. Wiggert, Mechanics of Fluids, Brooks/Cole, Pacific Grove, 2002.
[32] B.R. Manson, D.F. Young, T.H. Okiishi, Fundamentals of fluid mechanics, John Wiley & Sons, Toronto, 1990.
[33] I.H. Shames, Mechanics of Fluids, 4th ed., McGrawHill, New York, 2003.
[34] J.E. Finnemore, J.B. Franzini, Fluid Mechanics with Engineering Applications, 10th ed., McGrawHill, New York, 2002.
[35] R.W. Fox, Introduction to Fluid Mechanics, 4th ed., John Wiley & Sons, New York, 1994.
[36] C.O. Bennett, J.E. Meyers, Momentum, Heat and Mass Transfer, 3rd ed., McGrawHill Chemical Engineering Series, New York, 1982.
[37] F.M. White, Viscous Fluid Flow, 3rd ed., McGraw-Hill, Singapore, 2006.
[38] R.K. Shah, M.S. Bhatti, Laminar convective heat transfer in ducts, in: S. Kakaç, R.K. Shah, W. Aung (Eds.), Handbook of Single-Phase Convective Heat Transfer, John Wiley & Sons, New York, 1987pp. 3.1-3.31.
[39] P.H. Newell Jr., Laminar-flow heat transfer in horizontal tubes, PhD thesis Massachusetts Institute of Technology, Boston, 1966.
[40] T.V. Nguyen, Laminar heat transfer for thermally developing flow in ducts, Int. J. Heat Mass Transf. 35 (7) (1992) 1733–1741.
[41] S. Goldstein, Modern Developments in Fluid Dynamics, Oxford University Press, Oxford, 1938.
[42] B. Atkinson, Z. Kemblowski, J.M. Smith, Measurements of velocity profile in developing liquid flows, AIChE J. 13 (1) (1967) 17–20.
[43] A.F. Emery, C.S. Chen, An experimental investigation of possible methods to reduce laminar entry lengths, J. Basic Eng. 90 (1) (1968) 134–137.
[44] R.G. Deissler, Analytical and experimental investigation of adiabtic turbulent flow in smooth tubes, NACA TN 2138, NACA, Washington, 1950.
[45] Y.A. Cengel, A.J. Ghajar, Heat and Mass Transfer: Fundamentals and Applications, 5th ed., McGraw-Hill, 2015.

[46] A. Faghri, Y. Zhang, J.R. Howell, Advanced Heat and Mass Transfer, Global Digital Press, Columbia, 2010.
[47] J.C. Han, Analytical Heat Transfer, CRC Press, Boca Raton, 2016.
[48] P.S. Ghoshdastidar, Heat Transfer, 2nd ed., Oxford University Press, New Delhi, 2012.
[49] F.P. Keith, R.M. Manglik, Principles of Heat Transfer, 8th ed., Cengage Learning, Boston, 2018.
[50] R.K. Shah, Thermal entry length solutions for the circular tube and parallel plates, Third National Heat and Mass Transfer Conference, India Institute of Technology, Bombay, 1975, pp. 1–12.
[51] A.J. Salazar, A. Campo, Prediction of the thermal entry length without solving the complete entrance length problem, Int. J. Heat Fluid Flow 11 (1) (1990) 48–53.
[52] D.N. Roy, Development of laminar flow in circular and coaxial tubes with and without heat transfer, PhD thesis University of Calcutta, 1966.
[53] A.E. Bergles, R.R. Simonds, Combined forced and free convection for laminar flow in horizontal tubes with uniform heat flux, Int. J. Heat Mass Transf. 14 (12) (1971) 1989–2000.
[54] J.P. Meyer, M. Everts, Single-phase mixed convection of developing and fully developed flow in smooth horizontal circular tubes in the laminar and transitional flow regimes, Int. J. Heat Mass Transf. 117 (2018) 1251–1273.
[55] P.H. Newell Jr., A.E. Bergles, Analysis of combined free and forced convection for fully developed laminar flow in horizontal tubes, J. Heat Transfer 92 (1) (1970) 83–94.
[56] B. Metais, E. Eckert, Forced, mixed, and free convection regimes, J. Heat Transfer 86 (2) (1964) 295–296.
[57] M. Everts, J.P. Meyer, Flow regime maps for smooth horizontal tubes at a constant heat flux, Int. J. Heat Mass Transf. 117 (2018) 1274–1290.
[58] D. Oliver, The effect of natural convection on viscous-flow heat transfer in horizontal tubes, Chem. Eng. Sci. 17 (5) (1962) 335–350.
[59] T.M. Hallman, Combined free and forced convection in a circular tube, PhD thesis Purdue University, Lafayette, 1958.
[60] S. McComas, E. Eckert, Combined free and forced convection in a horizontal circular tube, J. Heat Transfer 88 (2) (1966) 147–152.
[61] R.L. Shannon, C.A. Depew, Combined free and forced laminar convection in a horizontal tube with a uniform heat flux, J. Heat Transfer 90 (3) (1968) 353–357.
[62] B.S. Petukhov, A.F. Polyakov, Experimental investigation of viscogravitational fluid flow in a horizontal tube, Teplofiz. Vysok. Temp 5 (1967) 87–95.
[63] K.C. Cheng, J.W. Ou, Free convection effects on Graetz problem for large Prandtl number fluids in horizontal tubes with a uniform wall heat flux, in: 5th International Heat Transfer Conference (IHTC-5), Tokyo, Japan, 1974, pp. 159-163.
[64] K.C. Cheng, S.W. Hong, G.J. Hwang, Buoyancy effects on laminar heat transfer in the thermal entrance region of horizontal rectangular channels with uniform wall heat flux for large Prandtl number fluid, Int. J. Heat Mass Transf. 15 (10) (1972) 1819–1836.
[65] S.W. Hong, S.M. Morcos, A.E. Bergles, Analytical and experimental results for combined forced and free laminar convection in horizontal tubes, 5th International Heat Transfer Conference (IHTC-5) (1974) 154–158.
[66] M. Everts, J.P. Meyer, Relationship between pressure drop and heat transfer of developing and fully developed flow in smooth horizontal circular tubes in the laminar, transitional, quasi-turbulent and turbulent flow regimes, Int. J. Heat Mass Transf. 117 (2018) 1231–1250.
[67] A.J. Ghajar, L.M. Tam, Laminar-transition-turbulent forced and mixed convective heat transfer correlations for pipe flows with different inlet configurations, in: Winter Annual Meeting of the American Society of Mechanical Engineers, ASME, New York, United States, 1991, pp. 15-23.
[68] A.J. Ghajar, K.F. Madon, Pressure drop measurements in the transition region for a circular tube with three different inlet configurations, Exp. Therm Fluid Sci. 5 (1) (1992) 129–135.
[69] A.J. Ghajar, L.M. Tam, Heat transfer measurements and correlations in the transition region for a circular tube with three different inlet configurations, Exp. Therm. Fluid Sci. 8 (1) (1994) 79–90.
[70] L.M. Tam, A.J. Ghajar, Effect of inlet geometry and heating on the fully developed friction factor in the transition region of a horizontal tube, Exp. Therm Fluid Sci. 15 (1) (1997) 52–64.
[71] H.K. Tam, L.M. Tam, A.J. Ghajar, S.C. Tam, T. Zhang, Experimental investigation of heat transfer, friction factor, and optimal fin geometries for the internally microfin tubes in the transition and turbulent regions, J. Enhanced Heat Transf. 19 (5) (2012) 457–476.
[72] H.K. Tam, L.M. Tam, A.J. Ghajar, Effect of inlet geometries and heating on the entrance and fully-developed friction factors in the laminar and transition regions of a horizontal tube, Exp. Therm Fluid Sci. 44 (2013) 680–696.
[73] L.M. Tam, A.J. Ghajar, The unusual behavior of local heat transfer coefficient in a circular tube with a bell-mouth inlet, Exp. Therm Fluid Sci. 16 (3) (1998) 187–194.
[74] J.A. Olivier, J.P. Meyer, Single-phase heat transfer and pressure drop of the cooling of water inside smooth tubes for transitional flow with different inlet geometries (RP-1280), HVAC R Res 16 (4) (2010) 471–496.
[75] G. Maranzana, I. Perry, D. Maillet, Mini- and micro-channels: influence of axial conduction in the walls, Int. J. Heat Mass Transf. 47 (17) (2004) 3993–4004.
[76] J.P. Meyer, S.M. Abolarin, Heat transfer and pressure drop in the transitional flow regime for a smooth circular tube with twisted tape inserts and a square-edged inlet, Int. J. Heat Mass Transf. 117 (2018) 11–29.
[77] C.O. Popiel, J. Wojtkowiak, Simple formulas for thermophysical properties of liquid water for heat transfer calculations [from O°C to 150°C], Heat Transfer Eng. 19 (3) (1998) 87–101.
[78] P.F. Dunn, Measurement and Data Analysis for Engineering and Science, 2nd ed., CRC Press, United States of America, 2010.
[79] M. Everts, Single-phase mixed convection of developing and fully developed flow in smooth horizontal circular tubes in the laminar, transitional, quasi-turbulent and turbulent flow regimes, PhD thesis University of Pretoria, Pretoria, 2017.
[80] S.M. Morcos, A.E. Bergles, Experimental investigation of combined forced and free laminar convection in horizontal tubes, J. Heat Transfer 97 (2) (1975) 212–219.
[81] F.M. White, Fluid Mechanics, 6th ed., McGraw-Hill, Singapore, 2009.